Article

Cell

A Serpin Shapes the Extracellular Environment to Prevent Influenza A Virus Maturation

Graphical Abstract

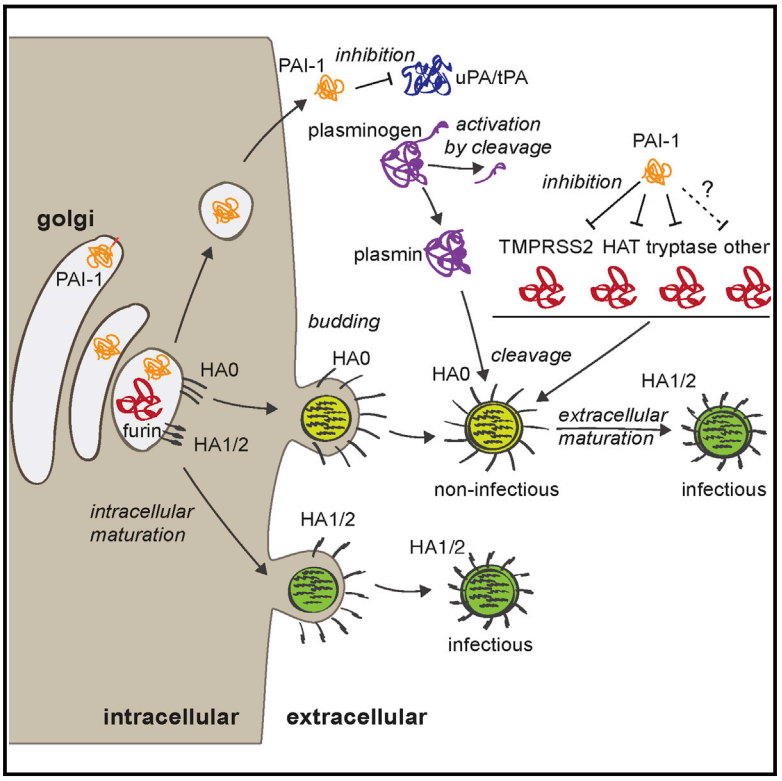

Highlights

- *SERPINE1*/PAI-1 was identified as an unconventional ISG that acts extracellularly
- PAI-1 inhibits influenza A virus (IAV) spread by inhibiting glycoprotein cleavage
- Endogenous PAI-1 blocks IAV spread in human and murine cells, ex vivo and in vivo
- PAI-1 potentially inhibits other viruses requiring extracellular maturation

Authors

Meike Dittmann,
Hans-Heinrich Hoffmann, ...,
Paul D. Bieniasz, Charles M. Rice

Correspondence

ricec@rockefeller.edu

In Brief

Plasminogen activator inhibitor (PAI-1) blocks surface glycoprotein maturation of influenza A virus, thus reducing virus spread in the airways and revealing that the innate immune system, driven by type I IFN, uses modulation of the extracellular environment to inhibit viruses.

Dittmann et al., 2015, Cell *160*, 631–643
February 12, 2015
http://dx.doi.org/10.1016/j.cell.2015.01.040

CellPress

Cell

A Serpin Shapes the Extracellular Environment to Prevent Influenza A Virus Maturation

Meike Dittmann,[1] Hans-Heinrich Hoffmann,[1] Margaret A. Scull,[1] Rachel H. Gilmore,[1] Kierstin L. Bell,[1] Michael Ciancanelli,[2] Sam J. Wilson,[3,4] Stefania Crotta,[5] Yingpu Yu,[1] Brenna Flatley,[1] Jing W. Xiao,[1] Jean-Laurent Casanova,[2,6,7,8,9] Andreas Wack,[5] Paul D. Bieniasz,[3] and Charles M. Rice[1,*]

[1]Laboratory of Virology and Infectious Disease, The Rockefeller University, New York, NY 10065, USA
[2]St. Giles Laboratory of Human Genetics of Infectious Diseases, Rockefeller Branch, The Rockefeller University, New York, NY 10065, USA
[3]Howard Hughes Medical Institute, Laboratory of Retrovirology, Aaron Diamond AIDS Research Center, The Rockefeller University, New York, NY 10016, USA
[4]Institute of Infection, Immunity and Inflammation, College of Medical, Veterinary and Life Sciences, University of Glasgow, Glasgow G12 8TA, UK
[5]Division of Immunoregulation, MRC National Institute for Medical Research, Mill Hill, London NW7 1AA, UK
[6]Howard Hughes Medical Institute, NY 10065, USA
[7]Laboratory of Human Genetics of Infectious Diseases, Necker Branch, Imagine Institute, Inserm, 75015 Paris, France
[8]Paris Descartes University, 75015 Paris, France
[9]Pediatric Hematology-Immunology Unit, Necker Hospital for Sick Children, 75015 Paris, France
*Correspondence: ricec@rockefeller.edu
http://dx.doi.org/10.1016/j.cell.2015.01.040

SUMMARY

Interferon-stimulated genes (ISGs) act in concert to provide a tight barrier against viruses. Recent studies have shed light on the contribution of individual ISG effectors to the antiviral state, but most have examined those acting on early, intracellular stages of the viral life cycle. Here, we applied an image-based screen to identify ISGs inhibiting late stages of influenza A virus (IAV) infection. We unraveled a directly antiviral function for the gene *SERPINE1*, encoding plasminogen activator inhibitor 1 (PAI-1). By targeting extracellular airway proteases, PAI-1 inhibits IAV glycoprotein cleavage, thereby reducing infectivity of progeny viruses. This was biologically relevant for IAV restriction in vivo. Further, partial PAI-1 deficiency, attributable to a polymorphism in human *SERPINE1*, conferred increased susceptibility to IAV in vitro. Together, our findings reveal that manipulating the extracellular environment to inhibit the last step in a virus life cycle is an important mechanism of the antiviral response.

INTRODUCTION

As obligate intracellular parasites, the fate of viruses is intricately linked to the metabolism of their host cells. Viruses exploit host cell mechanisms throughout their life cycle, from entry to replication, assembly and egress, and finally maturation. Each step in this cycle is a potential point for antiviral intervention.

Virus-infected cells produce interferons (IFNs) that trigger transcriptional upregulation of IFN-stimulated genes (ISGs) (reviewed in Schneider et al., 2014). The combined action of hundreds of expressed ISG proteins creates multiple lines of defense against viral infection. It is not surprising that different ISGs block different pathways and have varying potency against different classes of viruses (Schoggins et al., 2014). Our knowledge of ISG effector functions has been somewhat biased toward inhibition of early replication stages, such as entry, or viral translation initiation. However, viral assembly and release have proven to be an Achilles heel for viruses and are the targets of therapeutic small molecules (influenza A virus [IAV] neuraminidase inhibitors; HIV-1 protease inhibitors) and intrinsic ISGs such as tetherin (Neil et al., 2008) or viperin (Wang et al., 2007).

In this study, we established a screen that would also uncover host factors inhibiting late stages of the viral replication cycle, using IAV as a model virus. Applying an approach that accurately monitors several rounds of viral replication in the presence of single overexpressed ISGs, we discovered a direct antiviral function of the well-known gene *SERPINE1*, which encodes PAI-1 (Ny et al., 1986). We demonstrate that PAI-1 inhibits IAV maturation by targeting host proteases needed for viral glycoprotein cleavage and that this is physiologically relevant in natural proteolytic landscapes both in vitro and in vivo. Finally, we link a human genetic polymorphism in extracellular PAI-1 production to enhanced IAV susceptibility in vitro. In all, we show that shaping the extracellular environment can be a powerful mechanism in the vast arsenal of the innate immune response against invading pathogens.

RESULTS

A Gain-of-Function Screen Reveals *SERPINE1* Encoding PAI-1 as an Inhibitor of IAV Spread

To identify ISG effectors targeting late stages of the IAV life cycle, we established a high-throughput, image-based screen using an extended version of a recently published ISG library comprising 401 cDNAs (Schoggins et al., 2011; Table S1). Human lung adenocarcinoma cells (A549) were transduced with lentiviral vectors to express individual ISGs (Figure 1A). After 48 hr, cells were challenged with IAV WSN/33 (H1N1) at an MOI of 0.01.

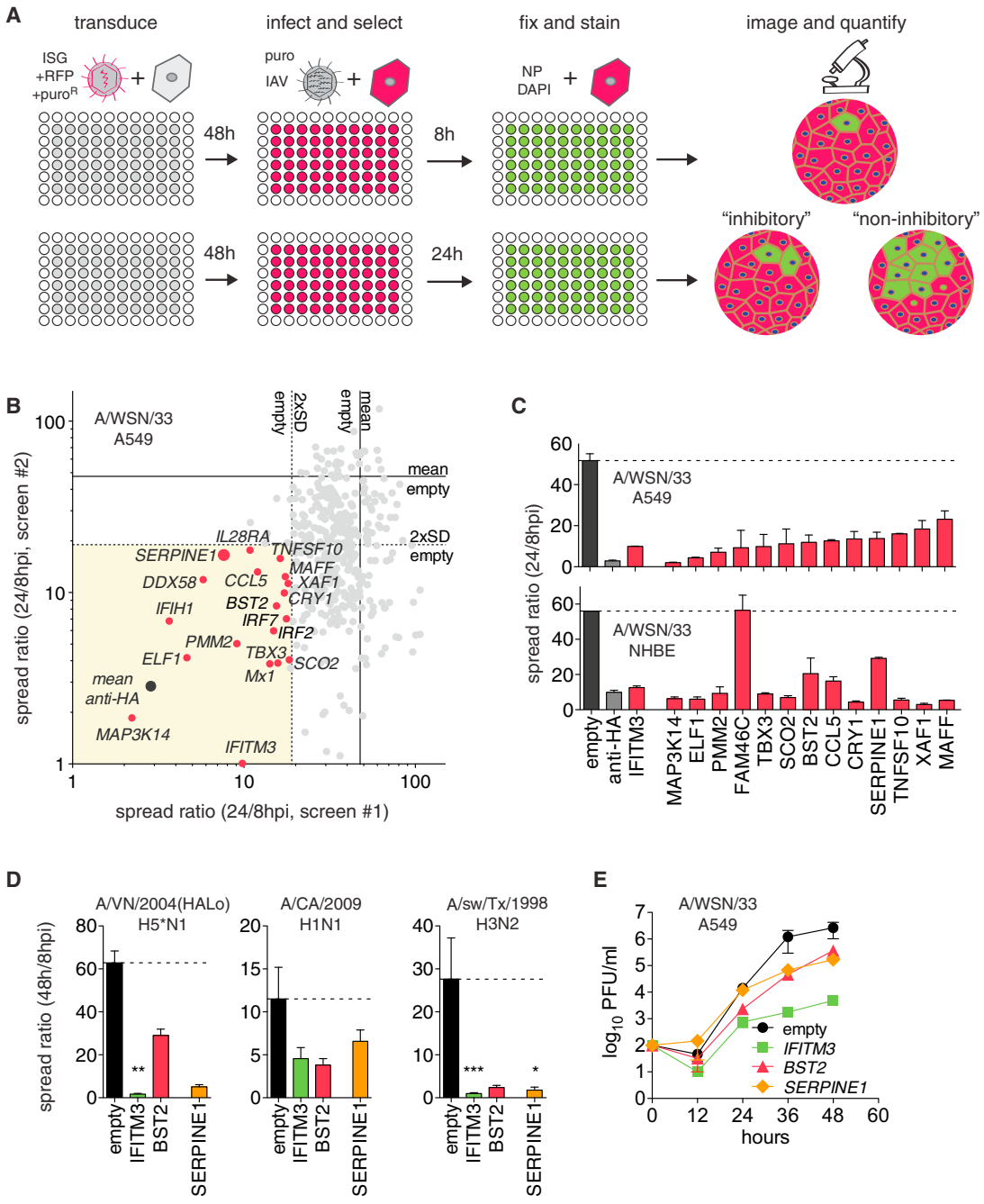

Figure 1. High-Throughput Microscopy Screens for Inhibitors of IAV Spread

(A) Screening workflow. Shown are hypothetical effects of expressing inhibitory (antiviral) or non-inhibitory ISGs on single or multiple rounds of virus replication. Red, transduced cells; green, infected cells; blue, DAPI-stained nuclei.

(B) Effect of 401 single ISGs on IAV spread. ISGs inhibiting more than 2-fold SD in two independent screens are shown in red. Spread ratio, the ratio of infected cells at 24/8 hpi. A positive control for inhibition is α-HA antibody.

(C) Confirmation assays for selected ISGs on A549 cells or primary NHBE cells. Data are represented as mean ± SEM from n = 6 values in two independent experiments for A549, and n = 3 for NHBE cells.

(D) *SERPINE1*(PAI-1)-mediated inhibition of A/Vietnam/1203/2004(HALo), A/California/04/2009, and A/sw/Texas/4199-2/1998 in A549 cells. Empty vector, negative control; *IFITM3* and *BST2* (tetherin), positive controls. Data are represented as mean ± SEM from n = 4 independent experiments. One-way ANOVA and Dunn's multiple comparison test versus "empty."

(E) ISG-expressing A549 cells were infected with IAV WSN/33 at MOI 0.01, and virus titers were measured by plaque assay on MDCK cells. Data are represented as mean ± SEM from n = 4 independent experiments.

See also Figure S1.

"Spread ratio" was calculated from the number of infected cells at 24 hr post-infection (hpi) relative to 8 hpi for each ISG (Figures 1A and S1A).

The screen was performed twice, using independently generated lentivirus libraries (Figure 1B). α-HA antibody, with a spread ratio of ~2, was a positive control, whereas empty vector controls had a spread ratio of 50 to 60 (Figures S1C and 1B). Nineteen ISGs reduced the IAV spread ratio to <20, greater than two SDs from the empty vector control in both screens (Figure 1B and Table S2). Among these ISGs were several broadly acting antiviral factors involved in pattern recognition and IFN signaling, such as *DDX58* (RIG-I), *IFIH1* (MDA5), *IRF2*, *IRF7*, *IL28RA* (IFNLR1), inflammatory cytokines, *CCL5* (RANTES), and broadly acting or IAV-specific inhibitors, such as *IFITM3*, *Mx1*, and *BST2* (Schneider et al., 2014). *IFITM3* and *Mx1* act early (IAV entry or replication), whereas *BST2*, also known as tetherin, prevents release of budding virus particles at the host cell surface. Although conflicting data exist on IAV inhibition by tetherin (Mangeat et al., 2012; Watanabe et al., 2011; Yondola et al., 2011), it potently inhibited spread in A549 cells and was subsequently used as a positive control. We also identified a number of ISGs with previously uncharacterized antiviral activities: *MAP3K14*, *ELF1*, *PMM2*, *FAM46C*, *TBX3*, *SCO2*, *CRY1*, *TNFSF10* (TRAIL), *XAF1*, *MAFF*, and *SERPINE1* (serine protease inhibitor, member E1). We validated this set of genes with independently generated, high-titer lentiviral stocks and A549 cells, as well as normal human bronchial epithelial cells (NHBE). All but *FAM46C*, which did not inhibit virus spread on NHBE cells, were confirmed as antiviral (Figure 1C). To exclude false positives due to cytotoxicity, we tested cell proliferation, apoptosis, DNA damage, and cell death profiles by high-throughput microscopy (HTM) (Figure S1D). We found that only expression of *MAP3K14*, the most potent hit in our screen, and *TNFSF10* were cytotoxic relative to the empty vector control.

Because protease inhibitors have been used clinically to treat other viruses (e.g., HIV), an endogenous effector with a similar function was a promising lead. We therefore focused on exploring the antiviral action of *SERPINE1*, encoding PAI-1. *SERPINE1* expression inhibited spread of various clinical IAV isolates, including a derivative of a highly pathogenic avian H5 influenza virus, modified to remove the polybasic cleavage site in the viral hemagglutinin (Steel et al., 2009), A/Vietnam/1203/2004(HALo) (H5N1), the pandemic A/California/04/2009 (H1N1), and an isolate of swine origin, A/sw/Texas/4199-2/1998 (H3N2) (Figure 1D). In multi-step viral growth kinetics, *SERPINE1* expression reduced extracellular IAV WSN/33 titers ~10-fold, comparable to inhibition by tetherin (Figure 1E).

This versatile SERPIN family member has been implicated in many physiological processes, including regulation of fibrinolysis (reviewed in Declerck and Gils, 2013). However, since an antiviral effector function of PAI-1 protein in the context of the intrinsic immune response is novel, we set out to determine its role in restricting IAV infection.

IAV Infection Enhances Secretion of PAI-1, which Is Both Necessary and Sufficient for IAV Inhibition

We first studied the kinetics of *SERPINE1* gene expression, as well as PAI-1 protein production and secretion. We compared A549 cells and the more relevant in vitro model of NHBE-derived, differentiated human ciliated airway epithelium cultures (HAEC), which mimic both the morphology and physiology of the airway epithelium in vivo. In A549 cells, *SERPINE1* mRNA was slightly upregulated upon IFN-β stimulation and following infection with IAV WSN/33 (Figure 2A). This was not due to nonresponsiveness of A549 cells, since other ISGs were highly upregulated (Figures S2A–S2C). TGF-β is known to trigger *SERPINE1* expression via the canonical Wnt/β-catenin pathway (He et al., 2010). Indeed, TGF-β treatment of A549 cells strongly induced *SERPINE1* expression with no or modest effects on *ISG15*, *IFITM3*, and *BST2* mRNA levels (Figures S2A–S2D). Stimulation of *SERPINE1* gene expression led to increased intracellular and extracellular levels of PAI-1 (Figures 2B, 2C, S2E, and S2F). Consistent with PAI-1 being efficiently secreted, total PAI-1 levels in the supernatant were about 16-fold higher than in respective IFN-β-treated cell lysates at 24 hr (Figures 2B and 2C). We observed apical secretion of PAI-1 by HAEC after either IAV WSN/33 infection (Figure 2D) or TGF-β treatment (Figure S2G). Of note, even mock-treated A549 cells and HAEC constantly produced and secreted basal levels of PAI-1 that accumulated over time (Figures 2B–2D). However, PAI-1 is further upregulated by certain stimuli, including virus infection.

To test possible IAV inhibition by extracellular PAI-1, we added recombinant active PAI-1 (rPAI-1) to the supernatant of A549 cells during IAV infection. rPAI-1 decreased IAV WSN/33 spread in a dose-dependent manner (Figure 2E). Conversely, we used a polyclonal α-PAI-1 antibody that targets the α-helix F of PAI-1 to neutralize PAI-1's ability to inhibit proteases (Komissarov et al., 2005). Strikingly, we found that addition of α-PAI-1 antibody to A549 cells during infection significantly enhanced IAV spread compared to the IgG control (Figure 2E).

Thus far, the extracellular environment in our experiments was defined by components of the growth medium or by proteins secreted by the cultured cells (endogenous or overexpressed). To test the potency of PAI-1 in a more natural setting, we examined IAV growth kinetics on HAEC in the presence or absence of rPAI-1. Strikingly, addition of rPAI to the apical side of HAEC significantly reduced IAV growth compared to carrier control, with ~10-fold lower infectivity at 48 hpi (Figure 2F). In contrast, addition of α-PAI-1 antibody dramatically enhanced IAV growth as early as 12 hpi and continued throughout the course of infection. In both A549 cells and HAEC, human parainfluenzavirus 3 (HPIV3) was unaffected by either of these treatments, showing that the effect was selective for IAV and not due to cytotoxicity (Figures S2H and S2I).

Experiments probing which stage of the viral life cycle was affected by PAI-1 showed no effects on early stages, replication, or egress (Figures S3A–S3E). However, a reduction of progeny particle infectivity (Figure S3F), together with the extracellular presence of PAI-1 (Figure 2) and its well-described function as protease inhibitor (Declerck and Gils, 2013), led us to investigate this activity as the mechanistic basis of PAI-1-mediated IAV inhibition.

PAI-1 Targets Airway Proteases Needed for Extracellular IAV Maturation

Infectivity of IAV progeny particles requires a maturation cleavage of the viral hemagglutinin (HA0 to HA1 and HA2), catalyzed

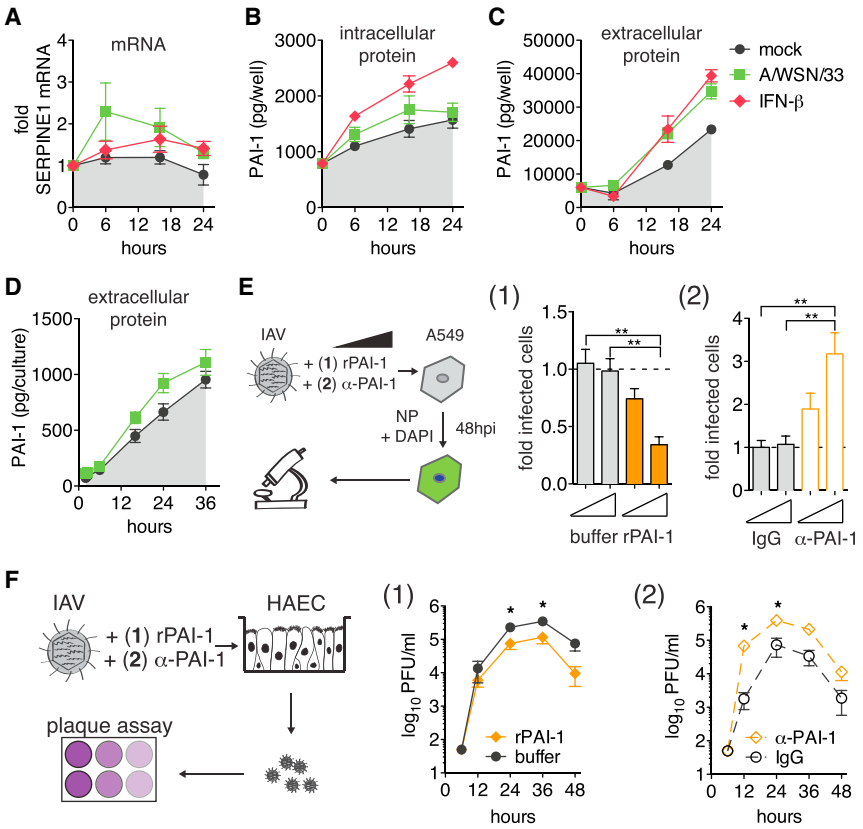

Figure 2. *SERPINE1* Gene Expression Profiles and the Role of Extracellular PAI-1 Protein for IAV Inhibition

(A–C) A549 cells were infected with IAV WSN/33, treated with IFN-β, or mock-treated. (A) *SERPINE1* mRNA expression was normalized relative to housekeeping gene *RPS-11*. Fold increase over pre-treatment control levels is shown. Accumulated total (B) intracellular and (C) extracellular protein levels of PAI-1 were determined by ELISA. Data are represented as mean ± SEM from n = 3 experiments.

(D) HAEC infected with IAV WSN/33 or mock treated. Accumulated PAI-1 protein in repeated apical washes was determined by ELISA. Data are shown as mean ± SEM from n = 3 replicates.

(E) A549 cells were infected with IAV WSN/33 in the presence of either rPAI-1 (1) or α-PAI-1 antibody (2), and virus spread was assayed by HTM at 48 hpi. The number of infected cells was normalized to buffer (1) or IgG (2). Data are represented as mean ± SEM from n = 4 independent experiments. Statistical significance relative to empty control was determined by t tests.

(F) HAECs were infected with IAV WSN/33 in the presence of either rPAI (1) or α-PAI-1 (2) and buffer (1) or IgG (2). Progeny virus was collected from apical washes, and rPAI-1 or α-PAI-1 were replenished after each wash. Virus titers were determined by plaque assay. Data are shown as mean ± SEM from n = 3 replicates.

See also Figure S2.

by host proteases (Lazarowitz and Choppin, 1975; Skehel and Waterfield, 1975). We tested whether known HA-cleaving proteases might be direct targets for PAI-1 inhibition. PAI-1 inhibits protease function by forming a covalent, SDS-stable bond with the target protease, detectable in gel shift assays. Urokinase plasminogen activator (uPA), a major target of PAI-1, formed a complex of ~85 kDa with rPAI-1, but not in the presence of the PAI-1 inhibitor triplaxtinin (Figure 3A). TPCK-trypsin is another established target of PAI-1 and a prototype chymotrypsin-like serine protease (Olson et al., 2001). To allow multiple rounds of IAV infection in cells lacking endogenous HA-cleaving proteases, such as A549, trypsin is typically added in low concentrations to the tissue culture medium. We readily detected PAI-1-trypsin complexes formed in vitro and their degradation products, which were again absent when triplaxtinin was added (Figure 3B). Furthermore, we identified human tryptase and human airway trypsin (HAT) as PAI-1 targets (Figures 3C and 3D). In contrast, we were unable to detect complexes of PAI-1 and furin, although this interaction has been previously reported (Figure S4) (Bernot et al., 2011).

The use of host proteases for maturation is not unique to IAV. Paramyxoviruses also use airway proteases to cleave their surface fusion (F) glycoprotein, and Sendai virus (SeV) utilizes the same extracellular airway proteases as IAV (Tashiro et al., 1992). In contrast, HPIV3 F is cleaved intracellularly by ubiquitous endoproteases such as furin. Using the spread assay and trypsin as protease, we found that HPIV3 was not inhibited by PAI-1, whereas IAV WSN/33 and SeV both exhibited reduced spread (Figures 3E–3G). *SERPINE1** encodes a catalytically inactive PAI-1 due to a single point mutation in the reactive center loop and served as a loss-of-function negative control (Lawrence et al., 1994). These data clearly demonstrate that PAI-1 targets trypsin-like airway proteases needed for extracellular virus maturation.

PAI-1 Prevents HA Cleavage of IAV Progeny Particles

Next, we examined the efficiency of HA cleavage in the presence of PAI-1 and trypsin. We found that rPAI-1 completely blocked trypsin-mediated cleavage of HA0 into HA1 and HA2 (Figure 4A). Furthermore, expression of wild-type PAI-1, but not the inactive mutant, reduced the specific infectivity of IAV Puerto Rico/8/34 grown in the presence of trypsin (Figure 4B). We found similar results for the extracellular airway proteases transmembrane protease serine 2 (TMPRSS2) and HAT, both known HA-cleaving proteases (Hatesuer et al., 2013; Figure 4C). Treatment with additional trypsin prior to virus titration restored specific infectivity to the level of virus grown in the presence of either protease, suggesting that the defect in specific infectivity was indeed caused by uncleaved HA (Figures 4B and 4C).

We next investigated cleavage efficiency of HA from different clades: H1 of A/Puerto Rico/8/34, H2 of A/Japan/305/57, and wild-type H5 of highly pathogenic A/Vietnam/1203/2004 (Figures 4D and 4E). Both $H1_{PR8}$ and $H2_{Japan}$ were uncleaved at baseline but were readily cleaved by either exogenous trypsin or overexpressed TMPRSS2 (Figure 4D).

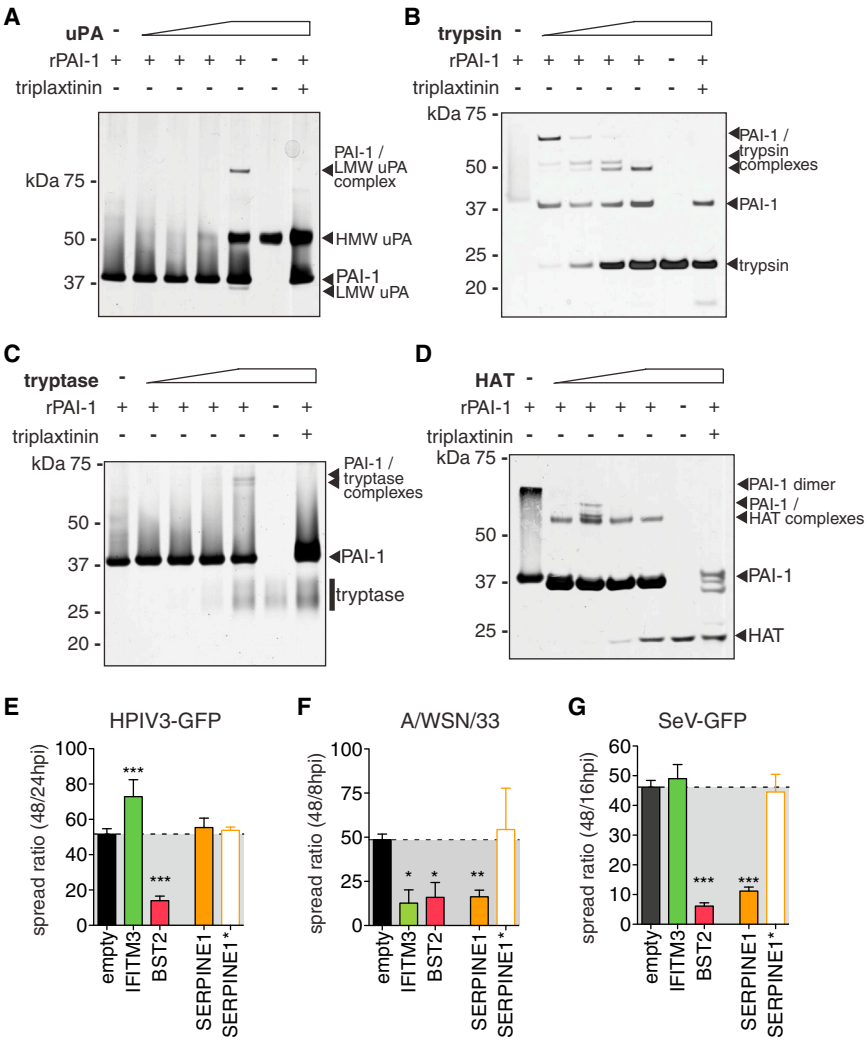

Figure 3. Protease Targets of PAI-1

(A–D) Representative gel shift assays to show complexes of recombinant PAI-1 (rPAI-1) and indicated proteases. 1 μg of rPAI-1 was combined with increasing amounts of protease, and the mixture was separated on SDS gels followed by silver staining. Where indicated, triplaxtinin was used to inhibit PAI-1 activity.

(E–G) HTM spread assay in the presence of PAI-1 wild-type (*SERPINE1*), loss-of-function mutant (*SERPINE1**), and controls for HPIV3-GFP (E), IAV WSN/33 (F), or SeV-GFP (G). Data are shown as mean ± SEM from at least n = 6 replicates from 2 independent experiments. One-way ANOVA and Kruskal-Wallis post-test.

See also Figure S4.

The slight differences in HA1 size between trypsin- and TMPRSS2-treated HA has been previously shown to be caused by altered glycosylation patterns in TMPRSS2-overexpressing cells (Bertram et al., 2010a). Further, we found that wild-type but not mutant PAI-1 inhibited TMPRSS2-mediated cleavage of both HA subtypes. In contrast, cleavage of $H5_{Vietnam}$, which is mediated by endogenous intracellular proteases such as furin, was not impaired by PAI-1 (Figure 4E). This result is in line with data from PAI-1-furin gel shift assays (Figure S4) and from experiments with furin-dependent HPIV3 (Figures S2H and S2I), further suggesting that furin is indeed not inhibited by PAI-1.

Finally, we examined the cleavage state of HA on HAEC. These cultures produce and secrete intrinsic airway proteases on their apical side; in fact, they have previously enabled identification of several proteases that cleave HA (Böttcher et al., 2006). Addition of rPAI-1 to HAEC during IAV WSN/33 infection dramatically reduced HA cleavage, whereas addition of α-PAI-1 increased cleavage (Figure 4F). These findings are in agreement with our previous results demonstrating virus growth kinetics in HAEC (Figure 2F).

Taken together, these data show that PAI-1 inhibits IAV spread by reducing extracellular cleavage maturation of progeny particles and that this mechanism operates in a physiologically relevant model of airway epithelium.

Serpine1$^{-/-}$ Mice Exhibit Enhanced IAV Infection and More Severe Disease Pathology

To examine the role of PAI-1 during IAV infection in vivo, we infected *Serpine1*$^{-/-}$ or *Serpine1*$^{+/+}$ (B6) control mice intranasally with IAVs Puerto Rico/8/34, WSN/33, or vesicular stomatitis virus (VSV) as a control. *Serpine1* was transcriptionally upregulated in B6 mouse lungs upon IAV infection (Figure 5B). We also detected increasing levels of murine PAI-1 (mPAI-1) in mouse lungs over the course of IAV infection with a 10-fold increase at 5 dpi compared to PBS-treated B6 (Figure 5C). Both *Serpine1* mRNA and mPAI-1 protein were undetectable in *Serpine1*$^{-/-}$ lung homogenates. IAV-infected *Serpine1*$^{-/-}$ mice exhibited significant weight loss and succumbed to infection on average 1 day earlier than B6 parental mice (Figures 5D, 5E, 5G, and 5H). This difference was not observed in mice infected with VSV control (Figure S5A). Despite the modest difference in survival, lung IAV titers at late times of infection were significantly elevated in *Serpine1*$^{-/-}$ (Figures 5F and 5I), which correlated with the levels of mPAI-1. Keller et al. (2006) used *Serpine1*$^{-/-}$ mice to study the effect of influenza virus infection on thrombosis, and they found no impact of PAI-1 on IAV infection, as measured by the amount of viral RNA at day 4 dpi. However, given the role of PAI-1 in blocking viral maturation, the levels of infectious virus particles (Figures 5F and 5I) are a more relevant measure. *Serpine*$^{-/+}$ mice exhibited an intermediate phenotype with respect to weight loss, survival, and murine lung PAI-1 levels, indicating a co-dominant effect of PAI-1 on IAV infection (Figure S5B).

Serpine1$^{-/-}$ lungs were increased in size at 5 days post-IAV infection, with enhanced necrosis compared to lungs from B6

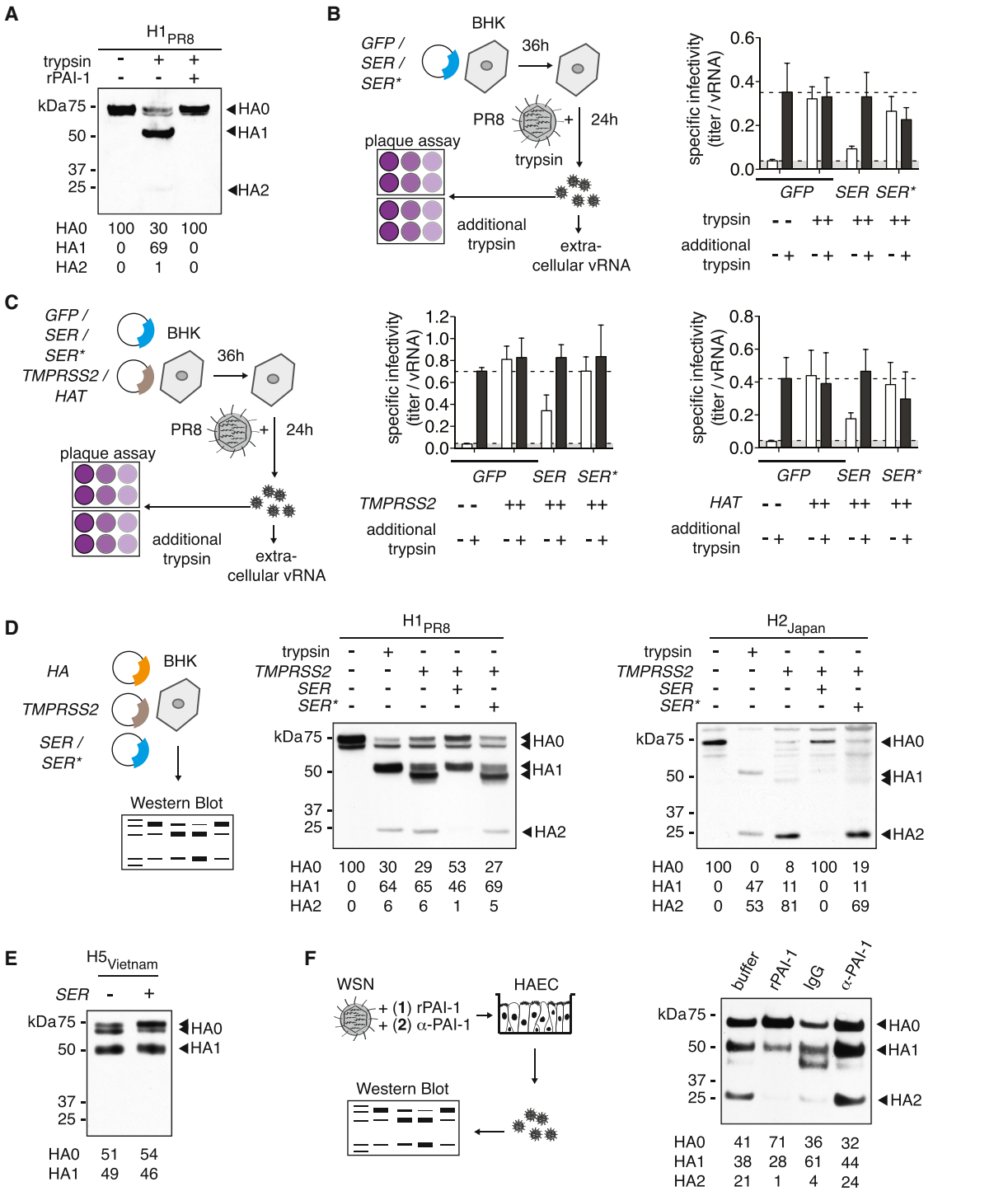

Figure 4. Effect of PAI-1 on Maturation of IAV HA

(A, D, and E) BHK cells were transfected in serum-free MEM to express HA of different origins. Whole-cell lysates were analyzed by western blot. HA cleavage products HA1 and HA2 are indicated, and relative band intensities are shown at the bottom of the gel.

(A) HA of A/Puerto Rico/8/34 origin. Shown are cells treated with TPCK-trypsin, TPCK-trypsin and rPAI-1, or buffer.

(B) BHK cells were transfected to express GFP as negative control, PAI-1 wild-type (*SER1*), or loss-of-function mutant (*SER**) and then challenged with IAV Puerto Rico/8/1934 in the presence of TPCK-trypsin. Supernatants were harvested and assayed for infectivity by focus forming assay on MDCK cells and for viral RNA by qRT-PCR. Plaque assays were performed in duplicate with or without additional post-harvest incubation with TPCK-trypsin. Specific infectivity was determined by calculating the ratio of FFU to vRNA copies, and values were normalized to GFP control. Data are shown as mean ± SEM from n = 6 replicates from 2 independent experiments.

(legend continued on next page)

controls (Figure 5A). Bleeding into alveoli was slightly enhanced in infected *Serpine1*$^{-/-}$ lungs at 4 dpi, which might be expected given PAI-1's role in fibrinolysis (Figure S5C). Cytokine expression was elevated in IAV-infected *Serpine1*$^{-/-}$ lungs compared to B6 control lungs, indicating increased inflammation (Figure S5D). In contrast, cytokine levels in uninfected lungs or in lungs from mice intranasally challenged with poly(I:C) were comparable between genotypes (Figure S5E). Thus, the increased weight loss and death observed in *Serpine1*$^{-/-}$ mice during IAV infection cannot be simply attributed to a global upregulation of cytokines. Whereas cytokine levels began to decrease in IAV-infected B6 lungs at 5 dpi, suggesting a subsiding infection, they stagnated in *Serpine1*$^{-/-}$ lungs, indicating an ongoing infection in *Serpine1*$^{-/-}$ mice. This correlated with the presence of higher IAV titers in *Serpine1*$^{-/-}$ mice at this late time point.

To further confirm the in vivo phenotype, we generated murine tracheal epithelial cultures (MTEC) from the trachea of *Serpine1*$^{-/-}$ or B6 wild-type mice, similar to HAEC. After challenge with A/X-31(H3N2), we found significantly increased vRNA and infectious virus in the *Serpine1*$^{-/-}$ cultures at later times of infection (Figure 5J). These results strengthen the physiological relevance of *Serpine1* as regulator of IAV spread and a component of the host barrier that restricts IAV infection in vivo.

Natural PAI-1 Deficiency in Human Fibroblasts Is Correlated with Increased Spread of IAV

Several single nucleotide polymorphisms (SNPs), often linked to bleeding disorders, have been described for *SERPINE1* (Fay et al., 1997; Zhang et al., 2005). SNP rs6092 is located in the signal peptide sequence of *SERPINE1* (c.A43T), resulting in substitution of alanine by threonine (PAI-1 p.A15T) and partial intracellular retention of PAI-1. In fact, a heterozygous rs6092 carrier had 30% reduced serum PAI-1 and a tendency to hemorrhage (Zhang et al., 2005). We characterized IAV susceptibility in three human fibroblast lines with at least one rs6092 allele. Two of these are heterozygous for *SERPINE1* c.A43T (designated as T/A 4 and 5, Figure 6), and one is homozygous (A/A 6). We compared them to three control lines, all encoding wild-type PAI-1 (T/T 1-3).

We found that IAV WSN/33 spread was significantly enhanced in the three c.A43T fibroblast lines compared to controls (Figures 6A and 6B). This was not due to enhanced replication, at least for T/A 5 and A/A 6 because the number of infected cells during one round of replication was similar to controls (Figure 6C). In multicycle growth experiments, we observed some variation between control lines, which is common, as donors are genetically heterogeneous. However, we found that each c.A43T fibroblast line produced significantly more infectious virus compared to each of the three controls (Figure 6D).

To determine whether this phenotype was selective for IAV, we challenged the fibroblasts with HPIV3. Indeed, two of our three c.A43T fibroblast lines, T/A 5 and A/A 6, did not support increased spread or replication of HPIV3, as determined by HTM, or in multicycle growth assays (Figures 6E–6G). However T/A 4 exhibited both enhanced HPIV3 spread and replication compared to controls, in which we had previously observed enhanced IAV replication (Figure 6C), suggesting that this cell line may have other properties unrelated to *SERPINE1* that promote virus replication and spread.

Extracellular PAI-1 levels of c.A43T fibroblast cultures were about 50% that of controls, which was consistent with previous reports (Figure 6H; Zhang et al., 2005). We next attempted to rescue IAV spread inhibition by adding rPAI-1 to the culture medium of A/A 1, T/A 5, and A/A 6 cells during IAV WSN/33 infection. rPAI-1 dramatically reduced virus spread in T/A 5 and A/A 6 cells down to the level of T/T 1 control cells in a dose-dependent manner. In contrast, control *STAT1*$^{-/-}$ fibroblasts, which support enhanced spread, but do not harbor c.A43T nor have reduced extracellular PAI-1 levels, could not be rescued to the level of T/T 1 controls (Figure 6I).

These results show that a natural extracellular PAI-1 deficiency correlates with increased IAV spread.

DISCUSSION

We identified the serine protease inhibitor PAI-1 as an ISG that restricted IAV spread, and we characterized its previously undescribed antiviral function. PAI-1 is a 50 kDa glycoprotein and the main physiological inhibitor of urokinase/tissue plasminogen activators (uPA/tPA), both major regulators of the fibrinolytic system. uPA/tPA convert the zymogen plasminogen into plasmin, triggering a proteolytic cascade to dissolve blood clots (reviewed in Declerck and Gils, 2013). PAI-1 is present in plasma, platelets, and the extracellular matrix and is secreted by endothelial, smooth muscle, and immune cells in different tissues, including the airway. Other than uPA/tPA, PAI-1 inhibits multiple serine proteases of the chymotrypsin type, with varying efficiencies (Irving et al., 2000).

Here, we find three new PAI-1 protease targets: human tryptase (tryptase Clara; club cell secretory protein), HAT, and TMPRSS2, all of which are involved in extracellular IAV glycoprotein cleavage. This finding suggests a role for PAI-1 as an antiviral factor by targeting extracellular maturation of IAV particles.

IAV maturation involves cleavage of its surface glycoprotein HA into HA1 and HA2. These proteins remain linked via a disulfide bond (Skehel and Waterfield, 1975), which forms a hinge, a prerequisite for viral envelope fusion during entry (Klenk et al., 1975; Lazarowitz and Choppin, 1975). Because IAV does not encode its own protease, HA cleavage depends on the

(C) BHK cells were transfected to co-express GFP as negative control, PAI-1 wild-type (*SER*), or loss-of-function mutant (*SER**), and TMPRSS2 or HAT as bait protease. Cells were then challenged, and virus infectivity was analyzed as described in (B).

(D) HA cleavage assay with H1 of A/Puerto Rico/8/34 or H2 of A/Japan/305/57 origin in the presence of protease TMPRSS2 and wild-type (*SER*) or loss-of-function (*SER**) PAI-1.

(E) HA cleavage assay with H5 of A/Vietnam/1203/2004 origin and wild-type (*SER*) PAI-1, or GFP as a negative control.

(F) HA cleavage assay on HAEC infected with IAV WSN/33 in the presence of either rPAI (1) or α-PAI-1 (2) and buffer (1) or IgG (2). Progeny virus particles from apical washes at 24 hpi were analyzed.

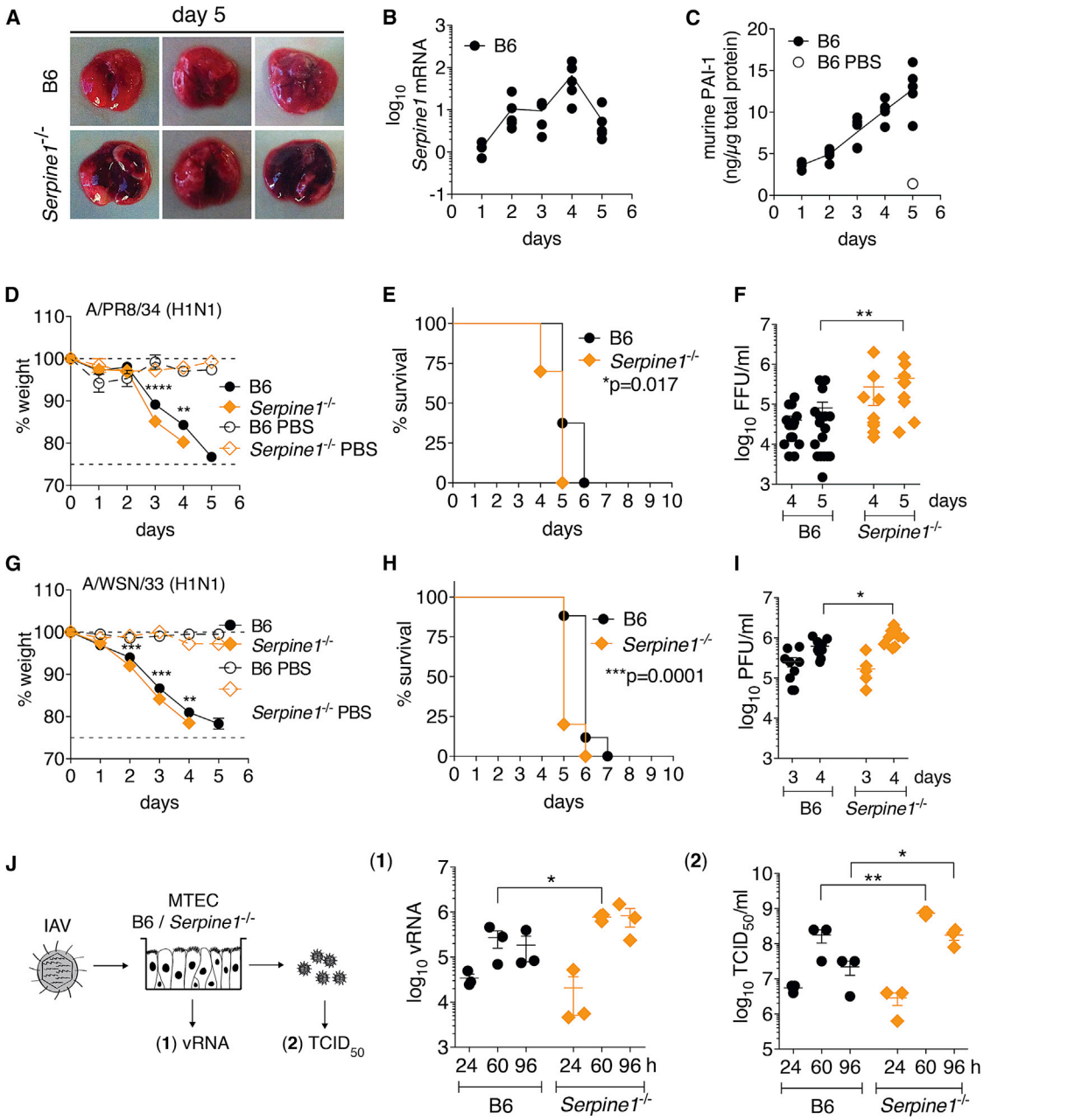

Figure 5. Role of *Serpine1* in Lethal IAV Infection in Mice

(A–F) Wild-type (B6) or *Serpine1*$^{-/-}$ mice were infected intranasally with 36 LD_{50} of IAV Puerto Rico/8/34. Statistical significance was determined by individual t tests (D, F, G, and I) or log rank test (E and H).

(A) Representative images of infected lungs 5 dpi.

(B and C) Homogenates of infected mouse lungs were assayed for *Serpine1* mRNA levels by qRT-PCR (B) and mPAI-1 protein levels by ELISA (C). Data are shown as mean ± SEM from n = 5 mice per group.

(D and E) Weight loss (D) and survival (E) of infected mice. Data are shown as mean ± SEM from n = 25 infected B6 or *Serpine1*$^{-/-}$ mice, and n = 3 respective PBS control animals.

(F) Homogenates of infected lungs were assayed for IAV titers by focus forming assay on MDCK cells. Data are shown as mean ± SEM from n = 17 B6 and 11 *Serpine1*$^{-/-}$ mice per day.

(G–I) Wild-type (B6) or *Serpine1*$^{-/-}$ mice were infected intranasally with 36 LD_{50} of IAV WSN/33 and monitored for weight loss (G) and survival (H). Data are shown as mean ± SEM from n = 32 infected B6 or *Serpine1*$^{-/-}$ mice, and n = 3 respective PBS control animals. IAV lung titers (I) shown as mean ± SEM from n = 9 B6 or *Serpine1*$^{-/-}$ mice per day.

(legend continued on next page)

presence of host proteases at the site of IAV replication. Furin and PC5/6, members of the subtilisin-like family of serine-proteases, are known to cleave HA intracellularly (Horimoto et al., 1994; Stieneke-Gröber et al., 1992). We could not find evidence for inhibition of furin by PAI-1. Human tryptase, HAT, TMPRSS2, TMPRSS13, mosaic serine protease large-form (MSPL), matrix metalloproteinase 9 (MMP9), and plasmin are known extracellular HA-cleaving proteases (Lazarowitz et al., 1973; reviewed in Bertram et al., 2010b). Most are members of the chymotrypsin-like serine protease family, the "target family" of PAI-1. Here, we provide direct proof that PAI-1 efficiently inhibits trypsin- and TMPRSS2-mediated cleavage of HA, and we hypothesize that PAI-1 might inhibit other members of this protease family as well.

Accessibility to glycoprotein cleavage is a major determinant of IAV pathogenicity (Bosch et al., 1981). Whether, and at what efficiency, an HA subtype can be cleaved by a given protease is determined by its cleavage site sequence. Highly pathogenic avian H5 and H7 HAs contain a multi-basic cleavage site, which makes them accessible to ubiquitiously expressed, intracellular proteases like furin (Bosch et al., 1981). Hence, viral particles of these subtypes are immediately mature and infectious upon budding. Less pathogenic IAV HAs, in contrast, contain a single arginine residue in their cleavage site, which makes them dependent on cleavage by extracellular airway proteases, such as TMPRSS2. Variation in the amino acid sequence surrounding this arginine alters cleavage efficiency (Galloway et al., 2013). Recent studies in *TMPRSS2*$^{-/-}$ mice revealed a direct influence on pathogenicity of IAV strains relying on this protease (Hatesuer et al., 2013; Sakai et al., 2014; Tarnow et al., 2014). In the absence of TMPRSS2, IAV of H1N1, H3N2, or H7N9 origin were unable to spread from the trachea to the lungs, making the mice highly resistant. This was not the case for highly pathogenic H5N1 virus (Sakai et al., 2014). Thus, sensitivity to PAI-1-mediated inhibition (or inhibition by other protease inhibitors) will depend on the nature of the cleaving protease, as well as on the cleavage efficiency of a specific HA subtype by that protease (Figure 5). In this regard, it will be interesting to determine whether the protease inhibitor PAI-1 has differential impact on pathogenicity of different IAV subtypes in vivo.

Not surprisingly, HA cleavage has been proposed as a target for antiviral therapy. Synthetic inhibitors, such as morpholinos or peptide mimetic protease inhibitors, have been used to target single proteases (Böttcher-Friebertshäuser et al., 2011). Leupeptin of actinomyces origin, the synthetic drug camostat, or aprotinin from bovine lungs all have broader antiprotease activity (Beppu et al., 1997; Lee et al., 1996; Tashiro et al., 1987; Zhirnov et al., 2011). So does recombinant mucus protease inhibitor (MPI), the only previously known airway protease inhibitor of human origin with anti-IAV activity (Beppu et al., 1997). The efficacy of applying these molecules to restrict IAV has been demonstrated both in vitro and in vivo and validates HA cleavage inhibition as an attractive antiviral strategy. Our data show that PAI-1 employs this mechanism and is the first known host protease inhibitor that functions to protect the host during natural IAV infection.

PAI-1 is a somewhat unconventional ISG, as it is constitutively expressed, but can be further upregulated by IFN and other cytokines like IL-6, IL-1, TGF-β, and TNF-α (Medcalf, 2007). This is significant because HA-cleaving proteases are often upregulated by IAV infection, skewing the protease-protease inhibitor balance in favor of the virus (Kido et al., 2012). Thus, PAI-1 may tip the balance back toward the host. Its regulation by TGF-β might be particularly relevant during IAV infections because IAV neuraminidase can activate latent TGF-β (Carlson et al., 2010). Other sources of TGF-β in the airway during infection include secretion by macrophages and by epithelial cells.

It is interesting that upregulation of *SERPINE1* gene expression during infection is not as dramatic as for other ISGs, possibly reflecting PAI-1's critical role in other local and systemic physiological processes, where massive overproduction could be deleterious for blood clotting, cancer metastasis, or cell adhesion and migration (reviewed in Declerck and Gils, 2013). PAI-1 is the only SERPIN that spontaneously—and quickly—adopts a latent form in vivo, which provides a regulatory mechanism, both spatially and temporally (Berkenpas et al., 1995).

The respiratory tract is a major portal for virus entry into the body but is protected by a multilayered antiviral fence. Mucus acts as a physical extracellular barrier. Mucins and surfactant proteins in mucus trap and aggregate virus particles outside of cells or act as decoy receptors inhibiting early steps in the viral replication cycle (Hartshorn et al., 2006; Reading et al., 2008). Mucins are present in airways at constitutive levels but are upregulated during inflammation (Turner and Jones, 2009). We now add PAI-1 as an additional component of this extracellular barrier. PAI-1 is the first extracellular directly antiviral ISG, and its promiscuity suggests that it may also play an important role in host defense against other respiratory viruses that rely on this step in their life cycles.

Many virus families require a maturation cleavage of viral surface glycoproteins, generally realized by serine proteases. Some use virus-encoded proteases, such as picornaviruses or retroviruses (Brody et al., 1992; Lee et al., 1993). Others, such as paramyxoviruses, orthomyxoviruses, coronaviruses, filoviruses, or arenaviruses, rely on host proteases (Glowacka et al., 2011; Lenz et al., 2001; Skehel and Waterfield, 1975; Steinhauer and Plemper, 2012; Volchkov et al., 1998). All are potentially sensitive to inhibition of their activating proteases by host or pharmacological protease inhibitors. Indeed, we show that a single inhibitor, PAI-1, significantly inhibits spread of IAV and SeV. Further exploration of the virus—activating protease—host inhibitor troika may open new avenues for antiviral intervention and deepen our understanding of virus maturation and pathogenicity.

(J) MTECs cultured from B6 or *Serpine1*$^{-/-}$ mice were infected with A/X-31(H3N2) at MOI = 10^{-6}. vRNA was quantified from lysed MTEC by qRT-PCR. In parallel, infectious virus titers were determined by $TCID_{50}$ assay on MDCK cells. Data are shown as mean ± SEM from n = 3 B6 or *Serpine1*$^{-/-}$ MTECs. Statistical significance was determined by two-way ANOVA.
See also Figure S5.

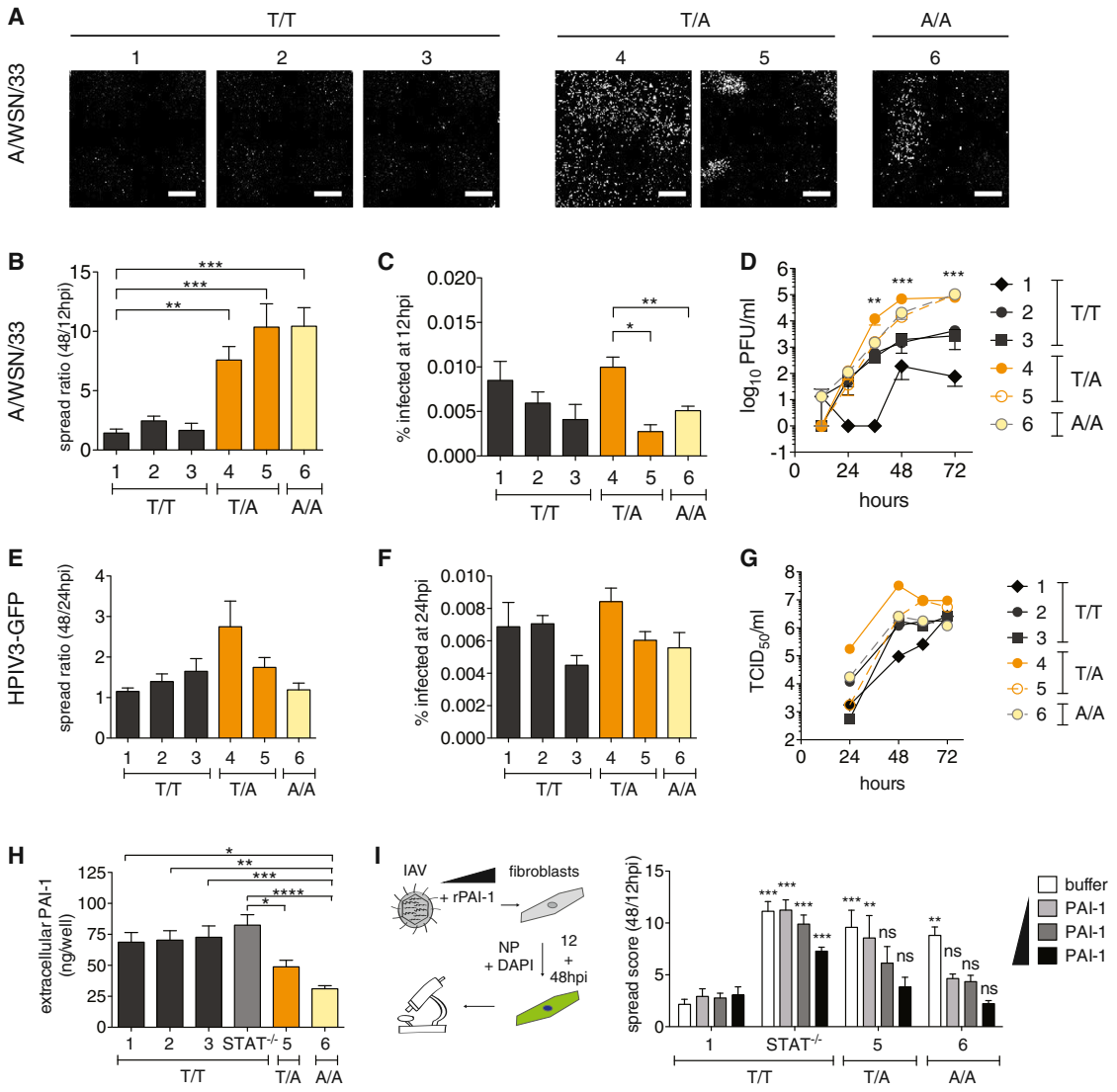

Figure 6. Susceptibility of PAI-1-Deficient Human Fibroblasts to IAV

(A–H) SV-40-immortalized human fibroblasts from different donors, wild-type (T/T 1-3), heterozygous (T/A 4 and 5), or homozygous (A/A 6) for *SERPINE1* SNP rs6092 were infected with IAV WSN/33 (A–D, H, and I) or HPIV3-GFP (E–G).

(A) Representative images from single wells infected with IAV WSN/33 at 48 hpi.

(B) IAV spread shown as the ratio between number of infected cells at 12/48 hpi.

(C) Percent of infected fibroblasts after one round of replication. Data in (A) and (B) are represented as mean ± SEM from n = 4 independent experiments, each in triplicate.

(D) IAV WSN/33 growth on fibroblasts. PFU in the supernatants were determined by plaque assay on MDCK cells. Data are represented as mean ± SEM from n = 4 independent experiments. Statistical significance was determined by individual t test, comparing the pooled SNP-carrying cells with the pooled control cells TT2 and TT3 for every time point.

(E) HPIV3-GFP spread shown as the ratio between number of infected cells at 48 and 24 hpi.

(F) Percent of infected fibroblasts after one round of replication. Data in (E) and (F) are represented as mean ± SEM from n = 2 independent experiments, each in triplicate.

(G) HPIV3-GFP growth on fibroblasts. $TCID_{50}$ in supernatants were determined on LLC-MK2 cells.

(H) Extracellular PAI-1 levels from IAV WSN/33-infected fibroblasts during spread assay at 48 hpi. Data are shown as mean ± SEM from total n = 8 replicates from n = 4 experiments.

(I) Rescue of virus inhibition on selected human fibroblast lines by adding rPAI-1 to the cultures during IAV WSN/33 infection. Maximum addition of rPAI-1 (black bars) was 500 ng, minimum addition (light gray bars) 125 ng. Data are represented as mean ± SEM from n = 4 independent experiments, each in quadruplicate. One-way ANOVA and Dunnett's multiple comparison post-test against T/T 1- values of the same condition.

In conclusion, we identify *SERPINE1*/PAI-1 as a host factor inhibiting IAV spread and show that PAI-1 mechanistically acts by blocking maturation of progeny IAV particles, thus reducing particle infectivity. Naturally occurring human genetic variations in PAI-1 impact the ability of IAV to spread from cell to cell, thus identifying PAI-1 as a candidate human gene that may influence susceptibility to IAV and the outcome of infection. In this regard, it will be of immediate interest to determine whether PAI-1 deficiency might be linked with the severity of human IAV infection. Finally, our work suggests that localized administration of PAI-1 to the respiratory tract might provide a new therapeutic approach for treating IAV and other respiratory viruses that require extracellular protease-driven maturation.

EXPERIMENTAL PROCEDURES

High-Throughput Microscopy Screening of Host Factor Library

Using Gateway technology, we transferred a previously published library of ISGs (Schoggins et al., 2011) from ORFEXPRESS entry clones into a new lentiviral expression vector (pSCRPSY), co-expressing TagRFP as a transduction control and puromycin resistance. A549 cells in 96-well plates were first transduced and then challenged with IAV WSN/33 at MOI 0.01. Due to varying transduction efficiency between the lentiviral stocks, the percentage of non-transduced cells was variable. IAV production from non-transduced cells masked potential inhibitory effects of ISGs and was eliminated by adding puromycin 1 hr prior to IAV infection. Lentiviral transduction was performed in duplicate plates for each ISG, where one sample was fixed after one round of replication (8 hpi), defining the number of initial producer cells, and the other after several rounds of replication (24 hpi). "Spread ratio" was calculated by dividing the IAV-infected cells at 24 hpi by 8 hpi for each individual ISG over empty vector-transduced cells (Figures 1A, S1A, and S1B) and yielded results that were stable over a wide range of transduction efficiencies (Figure S1B). Infected cells were detected by staining for IAV nucleoprotein (NP) and HTM (Figures 1A, S1A, and S1B).

Mice

Mice were housed in an AAALAC-accredited facility in accordance with the Guide for the Care and Use of Laboratory Animals. All procedures outlined in the study were approved by The Rockefeller University's Institutional Animal Care and Use Committee. Wild-type (C57BL/6J) and *Serpine*$^{-/-}$ (B6.129S2-Serpine$^{1tm1Mlg/J}$) breeder pairs were purchased from Jackson Laboratory, and colonies were established in-house. Six- to ten-week-old mice of both sexes were used in IAV challenge, and 10- to 14-week-old mice were used for VSV experiments.

Human Cell Lines

Informed consent was obtained from human subjects according to local regulations. Samples were subsequently transferred for experimental testing under respective ethics approvals at INSERM in France and at Rockefeller University in the USA. All protocols involving the use of human tissue were reviewed and exempted by The Rockefeller University Institutional Review Board.

SUPPLEMENTAL INFORMATION

Supplemental Information includes Extended Experimental Procedures, five figures, and three tables and can be found with this article online at http://dx.doi.org/10.1016/j.cell.2015.01.040.

AUTHOR CONTRIBUTIONS

H.-H.H. and M.A.S. contributed equally to this work. M.D. and C.M.R. designed the project. M.D. wrote the manuscript. M.D., H.-H.H., M.A.S., K.L.B., S.C., A.W., and C.M.R. designed the experiments. M.D., H.-H.H., M.A.S., R.H.G., K.L.B., B.F., Y.Y., S.C., and J.W.X. performed the experimental work. M.D., M.A.S., H.-H.H., S.J.C., and A.W. analyzed the results. S.J.W., M.C., A.W., P.D.B., and J.-L.C. contributed reagents and expertise.

ACKNOWLEDGMENTS

We would like to thank all Rice lab members but especially M. Hsu, M. Saeed, and Z. Ozair, for critical reading and helpful comments on the manuscript; Jeanne Chiaravalli-Giganti at the Rockefeller High-Throughput and Spectroscopy Resource Center and Sebastien Monettes at the Tri-Institutional Laboratory of Comparative Pathology for technical advice and support; Margaret MacDonald for VSV strain Indiana; Adolfo Garcia-Sastre for the gift of 2G9 α-HA antibody; Peter Palese for influenza viruses A/Puerto Rico/8/1934, A/Vietnam/1203/2004(HALo), A/California/04/2009, and A/sw/Texas/4199-2/1998; D. Steinhauer and S. Galloway for both the gift of pCAGGS-HA plasmids and for technical advice on the cleavage assay; Gary Whittaker for the gift of HAT and TMPRSS2 expression plasmids; and Sharmila Nair for advice with VSV in vivo experiments. This work was supported by National Institutes of Health (NIH) grant R01-AI091707 (C.M.R.), U54-AI057158 (I. Lipkin, Northeast Biodefense Center, subcontract to C.M.R.), the German Research Foundation and the Rockefeller Women and Science Fellowship (M.D.), Medical Research Council Grants U117597139 (to A.W. and S.C.), NIH grant 8UL1TR000043 from the National Center for Translational Sciences (NCATS; J.-L.C.), and the St. Giles Foundation (J.-L.C.). Additional funding was provided by the Greenberg Medical Research Institute, the Starr Foundation, and anonymous donors.

Received: September 19, 2014
Revised: October 22, 2014
Accepted: January 13, 2015
Published: February 12, 2015

REFERENCES

Beppu, Y., Imamura, Y., Tashiro, M., Towatari, T., Ariga, H., and Kido, H. (1997). Human mucus protease inhibitor in airway fluids is a potential defensive compound against infection with influenza A and Sendai viruses. J. Biochem. *121*, 309–316.

Berkenpas, M.B., Lawrence, D.A., and Ginsburg, D. (1995). Molecular evolution of plasminogen activator inhibitor-1 functional stability. EMBO J. *14*, 2969–2977.

Bernot, D., Stalin, J., Stocker, P., Bonardo, B., Scroyen, I., Alessi, M.C., and Peiretti, F. (2011). Plasminogen activator inhibitor 1 is an intracellular inhibitor of furin proprotein convertase. J. Cell Sci. *124*, 1224–1230.

Bertram, S., Glowacka, I., Blazejewska, P., Soilleux, E., Allen, P., Danisch, S., Steffen, I., Choi, S.Y., Park, Y., Schneider, H., et al. (2010a). TMPRSS2 and TMPRSS4 facilitate trypsin-independent spread of influenza virus in Caco-2 cells. J. Virol. *84*, 10016–10025.

Bertram, S., Glowacka, I., Steffen, I., Kühl, A., and Pöhlmann, S. (2010b). Novel insights into proteolytic cleavage of influenza virus hemagglutinin. Rev. Med. Virol. *20*, 298–310.

Bosch, F.X., Garten, W., Klenk, H.D., and Rott, R. (1981). Proteolytic cleavage of influenza virus hemagglutinins: primary structure of the connecting peptide between HA1 and HA2 determines proteolytic cleavability and pathogenicity of Avian influenza viruses. Virology *113*, 725–735.

Böttcher, E., Matrosovich, T., Beyerle, M., Klenk, H.D., Garten, W., and Matrosovich, M. (2006). Proteolytic activation of influenza viruses by serine proteases TMPRSS2 and HAT from human airway epithelium. J. Virol. *80*, 9896–9898.

Böttcher-Friebertshäuser, E., Stein, D.A., Klenk, H.D., and Garten, W. (2011). Inhibition of influenza virus infection in human airway cell cultures by an antisense peptide-conjugated morpholino oligomer targeting the hemagglutinin-activating protease TMPRSS2. J. Virol. *85*, 1554–1562.

Brody, B.A., Rhee, S.S., Sommerfelt, M.A., and Hunter, E. (1992). A viral protease-mediated cleavage of the transmembrane glycoprotein of Mason-Pfizer

monkey virus can be suppressed by mutations within the matrix protein. Proc. Natl. Acad. Sci. USA *89*, 3443–3447.

Carlson, C.M., Turpin, E.A., Moser, L.A., O'Brien, K.B., Cline, T.D., Jones, J.C., Tumpey, T.M., Katz, J.M., Kelley, L.A., Gauldie, J., and Schultz-Cherry, S. (2010). Transforming growth factor-β: activation by neuraminidase and role in highly pathogenic H5N1 influenza pathogenesis. PLoS Pathog. *6*, e1001136.

Declerck, P.J., and Gils, A. (2013). Three decades of research on plasminogen activator inhibitor-1: a multifaceted serpin. Semin. Thromb. Hemost. *39*, 356–364.

Fay, W.P., Parker, A.C., Condrey, L.R., and Shapiro, A.D. (1997). Human plasminogen activator inhibitor-1 (PAI-1) deficiency: characterization of a large kindred with a null mutation in the PAI-1 gene. Blood *90*, 204–208.

Galloway, S.E., Reed, M.L., Russell, C.J., and Steinhauer, D.A. (2013). Influenza HA subtypes demonstrate divergent phenotypes for cleavage activation and pH of fusion: implications for host range and adaptation. PLoS Pathog. *9*, e1003151.

Glowacka, I., Bertram, S., Müller, M.A., Allen, P., Soilleux, E., Pfefferle, S., Steffen, I., Tsegaye, T.S., He, Y., Gnirss, K., et al. (2011). Evidence that TMPRSS2 activates the severe acute respiratory syndrome coronavirus spike protein for membrane fusion and reduces viral control by the humoral immune response. J. Virol. *85*, 4122–4134.

Hartshorn, K.L., White, M.R., Tecle, T., Holmskov, U., and Crouch, E.C. (2006). Innate defense against influenza A virus: activity of human neutrophil defensins and interactions of defensins with surfactant protein D. J. Immunol. *176*, 6962–6972.

Hatesuer, B., Bertram, S., Mehnert, N., Bahgat, M.M., Nelson, P.S., Pöhlman, S., and Schughart, K. (2013). Tmprss2 is essential for influenza H1N1 virus pathogenesis in mice. PLoS Pathog. *9*, e1003774.

He, W., Tan, R., Dai, C., Li, Y., Wang, D., Hao, S., Kahn, M., and Liu, Y. (2010). Plasminogen activator inhibitor-1 is a transcriptional target of the canonical pathway of Wnt/beta-catenin signaling. J. Biol. Chem. *285*, 24665–24675.

Horimoto, T., Nakayama, K., Smeekens, S.P., and Kawaoka, Y. (1994). Proprotein-processing endoproteases PC6 and furin both activate hemagglutinin of virulent avian influenza viruses. J. Virol. *68*, 6074–6078.

Irving, J.A., Pike, R.N., Lesk, A.M., and Whisstock, J.C. (2000). Phylogeny of the serpin superfamily: implications of patterns of amino acid conservation for structure and function. Genome Res. *10*, 1845–1864.

Keller, T.T., van der Sluijs, K.F., de Kruif, M.D., Gerdes, V.E., Meijers, J.C., Florquin, S., van der Poll, T., van Gorp, E.C., Brandjes, D.P., Büller, H.R., and Levi, M. (2006). Effects on coagulation and fibrinolysis induced by influenza in mice with a reduced capacity to generate activated protein C and a deficiency in plasminogen activator inhibitor type 1. Circ. Res. *99*, 1261–1269.

Kido, H., Okumura, Y., Takahashi, E., Pan, H.Y., Wang, S., Yao, D., Yao, M., Chida, J., and Yano, M. (2012). Role of host cellular proteases in the pathogenesis of influenza and influenza-induced multiple organ failure. Biochim. Biophys. Acta *1824*, 186–194.

Klenk, H.D., Rott, R., Orlich, M., and Blödorn, J. (1975). Activation of influenza A viruses by trypsin treatment. Virology *68*, 426–439.

Komissarov, A.A., Andreasen, P.A., Bødker, J.S., Declerck, P.J., Anagli, J.Y., and Shore, J.D. (2005). Additivity in effects of vitronectin and monoclonal antibodies against alpha-helix F of plasminogen activator inhibitor-1 on its reactions with target proteinases. J. Biol. Chem. *280*, 1482–1489.

Lawrence, D.A., Olson, S.T., Palaniappan, S., and Ginsburg, D. (1994). Serpin reactive center loop mobility is required for inhibitor function but not for enzyme recognition. J. Biol. Chem. *269*, 27657–27662.

Lazarowitz, S.G., and Choppin, P.W. (1975). Enhancement of the infectivity of influenza A and B viruses by proteolytic cleavage of the hemagglutinin polypeptide. Virology *68*, 440–454.

Lazarowitz, S.G., Goldberg, A.R., and Choppin, P.W. (1973). Proteolytic cleavage by plasmin of the HA polypeptide of influenza virus: host cell activation of serum plasminogen. Virology *56*, 172–180.

Lee, W.M., Monroe, S.S., and Rueckert, R.R. (1993). Role of maturation cleavage in infectivity of picornaviruses: activation of an infectosome. J. Virol. *67*, 2110–2122.

Lee, M.G., Kim, K.H., Park, K.Y., and Kim, J.S. (1996). Evaluation of anti-influenza effects of camostat in mice infected with non-adapted human influenza viruses. Arch. Virol. *141*, 1979–1989.

Lenz, O., ter Meulen, J., Klenk, H.D., Seidah, N.G., and Garten, W. (2001). The Lassa virus glycoprotein precursor GP-C is proteolytically processed by subtilase SKI-1/S1P. Proc. Natl. Acad. Sci. USA *98*, 12701–12705.

Mangeat, B., Cavagliotti, L., Lehmann, M., Gers-Huber, G., Kaur, I., Thomas, Y., Kaiser, L., and Piguet, V. (2012). Influenza virus partially counteracts restriction imposed by tetherin/BST-2. J. Biol. Chem. *287*, 22015–22029.

Medcalf, R.L. (2007). Fibrinolysis, inflammation, and regulation of the plasminogen activating system. J. Thromb. Haemost. *5* (1), 132–142.

Neil, S.J.D., Zang, T., and Bieniasz, P.D. (2008). Tetherin inhibits retrovirus release and is antagonized by HIV-1 Vpu. Nature *451*, 425–430.

Ny, T., Sawdey, M., Lawrence, D., Millan, J.L., and Loskutoff, D.J. (1986). Cloning and sequence of a cDNA coding for the human beta-migrating endothelial-cell-type plasminogen activator inhibitor. Proc. Natl. Acad. Sci. USA *83*, 6776–6780.

Olson, S.T., Swanson, R., Day, D., Verhamme, I., Kvassman, J., and Shore, J.D. (2001). Resolution of Michaelis complex, acylation, and conformational change steps in the reactions of the serpin, plasminogen activator inhibitor-1, with tissue plasminogen activator and trypsin. Biochemistry *40*, 11742–11756.

Reading, P.C., Bozza, S., Gilbertson, B., Tate, M., Moretti, S., Job, E.R., Crouch, E.C., Brooks, A.G., Brown, L.E., Bottazzi, B., et al. (2008). Antiviral activity of the long chain pentraxin PTX3 against influenza viruses. J. Immunol. *180*, 3391–3398.

Sakai, K., Ami, Y., Tahara, M., Kubota, T., Anraku, M., Abe, M., Nakajima, N., Sekizuka, T., Shirato, K., Suzaki, Y., et al. (2014). The host protease TMPRSS2 plays a major role in in vivo replication of emerging H7N9 and seasonal influenza viruses. J. Virol. *88*, 5608–5616.

Schneider, W.M., Chevillotte, M.D., and Rice, C.M. (2014). Interferon-stimulated genes: a complex web of host defenses. Annu. Rev. Immunol. *32*, 513–545.

Schoggins, J.W., Wilson, S.J., Panis, M., Murphy, M.Y., Jones, C.T., Bieniasz, P., and Rice, C.M. (2011). A diverse range of gene products are effectors of the type I interferon antiviral response. Nature *472*, 481–485.

Schoggins, J.W., MacDuff, D.A., Imanaka, N., Gainey, M.D., Shrestha, B., Eitson, J.L., Mar, K.B., Richardson, R.B., Ratushny, A.V., Litvak, V., et al. (2014). Pan-viral specificity of IFN-induced genes reveals new roles for cGAS in innate immunity. Nature *505*, 691–695.

Skehel, J.J., and Waterfield, M.D. (1975). Studies on the primary structure of the influenza virus hemagglutinin. Proc. Natl. Acad. Sci. USA *72*, 93–97.

Steel, J., Lowen, A.C., Pena, L., Angel, M., Solórzano, A., Albrecht, R., Perez, D.R., García-Sastre, A., and Palese, P. (2009). Live attenuated influenza viruses containing NS1 truncations as vaccine candidates against H5N1 highly pathogenic avian influenza. J. Virol. *83*, 1742–1753.

Steinhauer, D.A., and Plemper, R.K. (2012). Structure of the primed paramyxovirus fusion protein. Proc. Natl. Acad. Sci. USA *109*, 16404–16405.

Stieneke-Gröber, A., Vey, M., Angliker, H., Shaw, E., Thomas, G., Roberts, C., Klenk, H.D., and Garten, W. (1992). Influenza virus hemagglutinin with multibasic cleavage site is activated by furin, a subtilisin-like endoprotease. EMBO J. *11*, 2407–2414.

Tarnow, C., Engels, G., Arendt, A., Schwalm, F., Sediri, H., Preuss, A., Nelson, P.S., Garten, W., Klenk, H.D., Gabriel, G., and Böttcher-Friebertshäuser, E. (2014). TMPRSS2 is a host factor that is essential for pneumotropism and pathogenicity of H7N9 influenza A virus in mice. J. Virol. *88*, 4744–4751.

Tashiro, M., Klenk, H.D., and Rott, R. (1987). Inhibitory effect of a protease inhibitor, leupeptin, on the development of influenza pneumonia, mediated by concomitant bacteria. J. Gen. Virol. *68*, 2039–2041.

Tashiro, M., Yokogoshi, Y., Tobita, K., Seto, J.T., Rott, R., and Kido, H. (1992). Tryptase Clara, an activating protease for Sendai virus in rat lungs, is involved in pneumopathogenicity. J. Virol. *66*, 7211–7216.

Turner, J., and Jones, C.E. (2009). Regulation of mucin expression in respiratory diseases. Biochem. Soc. Trans. *37*, 877–881.

Volchkov, V.E., Feldmann, H., Volchkova, V.A., and Klenk, H.D. (1998). Processing of the Ebola virus glycoprotein by the proprotein convertase furin. Proc. Natl. Acad. Sci. USA *95*, 5762–5767.

Wang, X., Hinson, E.R., and Cresswell, P. (2007). The interferon-inducible protein viperin inhibits influenza virus release by perturbing lipid rafts. Cell Host Microbe *2*, 96–105.

Watanabe, R., Leser, G.P., and Lamb, R.A. (2011). Influenza virus is not restricted by tetherin whereas influenza VLP production is restricted by tetherin. Virology *417*, 50–56.

Yondola, M.A., Fernandes, F., Belicha-Villanueva, A., Uccelini, M., Gao, Q., Carter, C., and Palese, P. (2011). Budding capability of the influenza virus neuraminidase can be modulated by tetherin. J. Virol. *85*, 2480–2491.

Zhang, Z.Y., Wang, Z.Y., Dong, N.Z., Bai, X., Zhang, W., and Ruan, C.G. (2005). A case of deficiency of plasma plasminogen activator inhibitor-1 related to Ala15Thr mutation in its signal peptide. Blood Coagul. Fibrinolysis *16*, 79–84.

Zhirnov, O.P., Matrosovich, T.Y., Matrosovich, M.N., and Klenk, H.D. (2011). Aprotinin, a protease inhibitor, suppresses proteolytic activation of pandemic H1N1v influenza virus. Antivir. Chem. Chemother. *21*, 169–174.

EXTENDED EXPERIMENTAL PROCEDURES

Viruses, Cells, and Plasmids

Egg-grown influenza viruses A/Puerto Rico/8/1934 (H1N1) (PR8), A/Vietnam/1203/2004(HALo) (H5N1), pandemic A/California/04/2009 (H1N1), and A/sw/Texas/4199-2/1998 (H3N2) were obtained from Peter Palese, and A/Puerto Rico/8/1934-NS1-GFP reporter virus was from Adolfo Garcia-Sastre. Human parainfluenza virus 3 – GFP (HPIV3-GFP) was a gift from Peter Collins, NIAID, NIH. We received Sendai virus-GFP from Dominique Garcin, University of Geneva. IAV WSN/33 (H1N1) and X-31(H3N2) were grown on MDCK cells. Vesicular stomatitis virus strain Indiana was grown and titrated on BHK cells. Adenocarcinomic human alveolar basal epithelial cells (A549), rhesus macaque kidney (LLC-MK2) and 293T cells were purchased from ATCC, and normal human bronchial/tracheal epithelial cells (NHBE) were from Lonza.

Human airway tracheobronchial epithelial cells isolated from airway specimens from patients with normal lungs were provided by Lonza, Inc. (Walkersville, MD). Primary cells derived from single patient sources were expanded on plastic to generate passage 1 cells, which were subsequently plated ($5x10^4$ cells/well) on rat-tail collagen type 1-coated permeable transwell membrane supports (6.5 mm; Corning Inc). HAE cultures were grown in B-ALI medium supplemented with inducer (Lonza, Inc.) at each media change with provision of an air-liquid interface for approximately 6 weeks to form differentiated, polarized cultures that resemble in vivo pseudostratified mucociliary epithelium.

For infection, HAE were rinsed with PBS to transiently remove apical secretions and supplied with fresh basolateral medium prior to inoculation. We used $5x10^4$ PFU A/WSN/33 or $1.4x10^4$ $TCID_{50}$ HPIV3-GFP, respectively, per culture. Virus was diluted in PBS and supplemented with either 5 ng rPAI-1, buffer (50 mM NaH_2PO_4, 100 mM NaCl, 1 mM EDTA, pH 6.6), 400 ng α-PAI-1 (abcam), or 400 ng rabbit IgG control per culture. The inoculum was applied to the apical surface of HAE for 2 hr at 37°C. Following incubation, viral inocula were removed, and cultures were washed 3 times with PBS. rPAI-1, buffer, α-PAI or IgG were replenished in 20 μl volume per culture, and cultures were incubated at 37°C for the duration of the experiment. Progeny virus was harvested at indicated times by performing apical washes with 100μl of PBS for 30 min at 37°C. After each wash, rPAI, buffer, α-PAI-1 or IgG were replenished. Washes were harvested and stored at −80°C prior to analysis. Viral titers in the apical washes were determined by plaque assay on MDCK cells (A/WSN/33), or $TCID_{50}$ assay on LLC-MK2 cells (HPIV3-GFP).

Primary human dermal fibroblasts were obtained from punch biopsies from human subjects from a cohort with various infectious disease. The cells were electroporated with a plasmid encoding the simian virus 40 (SV40) large T antigen to create SV40-immortalized fibroblasts (SV40-fibroblasts), and were maintained in DMEM (Invitrogen) supplemented with gentamycin and 10% FBS until primary cells were no longer present.

To screen ISGs for antiviral activity, we obtained sequence-validated ORFEXPRESS ISG shuttle clones (GeneCopoeia) and used Gateway technology to move genes into pSCRPSY lentiviral vector co-expressing RFP and a puromycin resistance gene. *SERPINE1* was cloned into pCR®8/GW/TOPO® TA (Life Technologies). This entry clone DNA was used as template to insert mutation T356R using Quikchange technology (Agilent). *SERPINE1* T356R (referred to as *SERPINE1**) was previously described to convey loss of function (Lawrence et al., 1994). Both *SERPINE1* wild-type and *SERPINE1** were moved into either pSCRPSY, for lentivirus production, or pDEST40 (Life Technologies), for transfection experiments.

$HA1_{PR8}$, $H2_{Japan}$ and $H5_{Vietnam}$ in pCAGGS-LIC were obtained from David Steinhauer (Emory University, Atlanta). Plasmids encoding TMPRSS2 and HAT were obtained from Gary Whittaker (Cornell University, Ithaca).

Antibodies, Stains, and Recombinant Proteins

For high-throughput microscopy, we used α-nucleoprotein (NP) mAb (Millipore), AnnexinV-AlexaFluor-647 conjugate (Life Technologies), anti-phosphorylated H2AX (Pierce), SYTOX green dead cell stain (Life Technologies), and AlexaFluor-488 or −647 secondary antibodies. To block spread of IAV in tissue culture, we used α-HA mAb 2G9 at 0.125 μg/ml (kind gift of Adolfo Garcia-Sastre). To neutralize PAI-1 in cell supernatants, we used rabbit polyclonal anti-PAI-1 (Abcam) at 50 or 10 μg/ml dilution, and rabbit IgG (Jackson Immunoresearch) as control. For visualization of HA in western blots, the following reagents were obtained through the NIH Biodefense and Emerging Infections Research Resources Repository, NIAID, NIH: Polyclonal anti-influenza virus H1 (H0) hemagglutinin (HA), A/Puerto Rico/8/34 (H1N1), antiserum, goat, NR-3148; polyclonal anti-influenza virus H2 hemagglutinin (HA), A/Singapore/1/1957 (H2N2), antiserum, goat, NR-4523; and polyclonal anti-influenza virus H5 hemagglutinin (HA), A/Vietnam/1203/2004 (H5N1), antiserum, goat, NR-2705.

We used recombinant active human PAI-1 (carrying stabilizing mutations N150K, K154T, Q319L and M354I, Abcam) in tissue culture at 25 or 12 ng/ml final concentration and in in vitro assays at 1 μg/reaction. TPCK trypsin, human tryptase (both Sigma), recombinant HAT (R&D Systems), recombinant active furin (Abcam and NEB), and recombinant active urokinase plasminogen activator (both Abcam) were used in a 1:2 serial dilutions starting at 1μg/reaction.

We used a stable form of rPAI-1, which carries four amino acid changes, prolonging its half-life from 2 to > 140 hr (Berkenpas et al., 1995). Target rPAI-1 levels in this experiment were chosen to reflect physiological concentrations, at 25 or 12.5 ng/ml, respectively.

High-Throughput Microscopy Screening of Host Factor Library

A549 cells in 96-well plates were transduced with the lentiviral ISG stocks for 2d, on duplicate plates, and then infected with IAV WSN/33 at 100 PFU/well (MOI 0.01). Puromycin selection of 10 μg/ml was applied from 60 min prior to IAV challenge until the end of the

experiment to suppress virus production from untransduced cells. To detect single round infection, cells were fixed with 1.5% paraformaldehyde at 8-12 hpi, and to monitor viral spread, duplicate wells were fixed at 24 hpi. Cells were then permeabilized with Triton X-100 (0.1% in PBS), and stained for NP-positive cells and DAPI. Fish gelatin (0.2% in PBS) was used as blocking reagent, and all washing steps during immunostaining were performed using BioTek EL406 Plate Washer and Dispenser. 48 overlapping images per well were taken using the ImageXPressMICRO System (Molecular Devices), and images were stitched and analyzed for total (DAPI), transduced (RFP) and infected cells (Alexa488) with MetaXPress software V5.1.0.46. 24hpi values were normalized to their respective early values to account for differences in transduction efficiency and to determine the number of cells that were infected at late stages from one initially infected cell ("founder cell"). For all ISG hit validation experiments, we generated lentiviral stocks that were independent from the primary screening preparations. When indicated in the respective figures, we modified the HTM protocol regarding cell type, virus and timing of time points.

ISG Induction Assays

To determine *SERPINE1* mRNA expression and protein secretion kinetics, we treated A549 cells or HAE cultures with the following conditions: IFN-β (Abcam) at 1pmol/ml, TGF-β (Abcam) at 1 pg/ml, IAV WSN/33 infection at MOI 1 (A549) or 0.1 (HAE). mRNA levels, normalized to housekeeping gene RPS-11, were determined by qRT-PCR (SuperScript III First Strand Synthesis System, Life Technologies) and SYBR green assay (Roche) as described previously. Primer sequences can be found in Table S3. Total PAI-1 protein levels from cell supernatants or cell lysates (1% Triton X-100 in PBS, sonication for 10 min) were measured by Human PAI-1 Platinum ELISA (BD Biosciences). mPAI-1 levels from mouse lung homogenates were measured by PAI-1 total mouse ELISA kit (Abcam).

Inhibitors

All inhibitors used in tissue culture were titrated for toxicity (by Sytox stain, AnnexinV stain, PrestoBlue assay) and subsequently used at the highest possible, non-cytotoxic dose. Diphyllin (ChemDiv) was used to block IAV entry at 10 μM, and Ribavirin at 500 μM as replication inhibition control, respectively. Triplaxtinin (PAI-039, Axonmedchem) was used as PAI-1 inhibitor for in vitro assays at 10 μM. JAK inhibitor 1 (Calbiochem) was used at 500 ng/ml in SeV-GFP spread assays.

Virus Infection Media

Unless stated otherwise, the following media was used during virus infections on A549 cells: DMEM, 0.3% BSA (Equitech), 0.1% FBS, Pen/Strep, 1 μg/ml TPCK-trypsin. For infection of human fibroblasts, we used DMEM, 0.3% protease-free BSA (Sigma), 0.1% FBS, Pen/Strep, and 1μg/ml TPCK-trypsin. For infection in serum-free conditions on BHK cells, MEM with Pen/Strep was used, with or without addition of 1 μg/ml TPCK, as indicated. We used serum-free overlay for plaque assay on MDCK cells: DMEM, 0.00001% DEAE, 0.0001% $NaHCO_3$, GlutaMax, NEAA, 0.5μg/ml TPCK, 1.2% avicel (or 1% oxoid agar).

IAV Life-Cycle Assays

We transduced A549 with the indicated lentiviruses, and performed all assays 2d after. For the mini genome assay, transduced cells were transfected, in a 24-well format, with pCAGGS constructs for IAV WSN/33 PB1, PB2, PA (100 ng each), and NP or empty pCAGGS (200ng), as well as the RNA polymerase II-driven Renilla luciferase reporter pRLTK (40 ng), and the IAV-specific RNA polymerase I-driven firefly luciferase reporter (pPolI-luc, 60 ng). Diphyllin or Ribavirin were added as controls 4h before transfection and until the end of the experiment. Cells were harvested 20h post-transfection, lysed and assayed using Dual Luciferase Assay Kit (Promega).

For determination of egress efficiency, transduced A549 were challenged with IAV WSN/33 at MOI 0.1. At 24 hpi, cells were harvested for quantitation of intracellular vRNA and supernatants for determination of extracellular vRNA and number of infectious particles. Viral RNA was extracted with RNeasy kit (QIAGEN, for cells) or QIAmp Viral RNA kit (QIAGEN, for supernatants). For genome quantification by Taqman RT-PCR we used RealTime ready RNA Virus Master (Roche); primer and probe sequences can be found in Table S3. The number of infectious particles in the supernatants were determined by plaque assay on MDCK cells using avicel overlay and crystal violet staining (A/WSN/33), or agar overlay followed by NP-immunostaining (A/PR/8/1934).

HA Cleavage and Specific Infectivity Assays

For HA cleavage assays with trypsin and rPAI, BHK cells were transfected in 6-well plates in serum-free MEM, with either 4 μg pCAGGS encoding HA_{PR8}. At 48h post-transfection, MEM was replaced by fresh MEM, MEM containing 5 μg/ml TPCK, or MEM containing a mix of 5 μg/ml TPCK and 20 μg/ml rPAI (previously incubated for 1h at 37°C). Cells were incubated for 60 min. Then, floating cells in media were collected by centrifugation, and remaining adherent cells were harvested with 1 ml/well of enzyme-free PBS-based dissociation reagent and scraping. For cleavage assays in the presence of TMPRSS2, BHK cells were transfected with 3 μg of respective HA plasmid, and 3 μg of SERPINE1/SERPINE1* plasmid plus 1 μg TMPRSS2 plasmid. At 48h post-transfection, 5 μg/ml trypsin were added to the control well for 30 min. Cells were then harvested by scraping, collected by centrifugation, and lysed in 1x NuPage loading buffer and reducing agent. HA cleavage was analyzed by western blot using antibody specific for the respective HA.

For specific infectivity assays, BHK cells were co-transfected, in MEM, with previously published protease-encoding plasmids (HAT or TMPRSS2) and pcDNA-DEST40 plasmids encoding PAI-1 wild-type or mutant T356R. At 36h post-transfection, media

was collected, cells were washed twice with PBS and infected in serum-free MEM with A/PR/8/1934 at MOI 0.5. After 1h of incubation, cells were washed again, and overlaid with the same media from before (containing PAI-1 and proteases). Supernatants were collected for plaque assay and vRNA at 24hpi. vRNA was determined by qRT-PCR, and FFU by focus forming assay. To rescue specific infectivity, a duplicate of supernatants was incubated with additional 2 μg/ml TPCK-trypsin in the dilution medium for 30 min prior to focus forming assay.

Mice

Wild-type (C57BL/6J; referred to as B6) and *Serpine*$^{-/-}$ mice were anesthetized with ketamine/xylazine (100 mg/10 mg/kg), and 36 LD_{50} IAV PR/8/1934 or WSN/33 virus, diluted in a volume of 35 μl, was administered intranasally. Dose-response experiments with PR8 and WSN in WT and KO mice had showed that 36 LD_{50} (corresponding 1000 PFU of PR8) was optimal to reveal the difference between WT and KO mice regarding weight loss, survival and viral titers. For VSV strain Indiana, 10^5 PFU per mouse were administered intranasally.

Clinical signs were assessed by visual inspection, as well as daily weighing of the animals. Animals that became moribund and lost > 25% of their body weight as compared to day 0 were immediately euthanized.

For the poly(I:C) challenge experiment, mice were anesthetized with ketamine/xylazine (100 mg/10 mg/kg), and 100 μg of poly(I:C) (InVivogen), diluted with PBS in a volume of 35 μl, was administered intranasally.

For determination of virus lung titers and ISG mRNA profiles, animals were sacrificed at indicated time points, whole lungs were collected, homogenized in 500 μl PBS, and debris was spun down at 15,000 rpm for 10 min. Supernatants were analyzed by plaque assay and qRT-PCR. Primer sequences for mouse ISG SYBR green assays can be found in the Table S3.

For pathology, following euthanasia by CO_2 inhalation, the chest was opened and 10% neutral buffered formalin (NBF) was injected in the trachea with a syringe and a 25 g needle until the lungs were expanded to their normal in situ size. The lungs were then immersed in 10% NBF, and 72h later were processed in ethanol and xylene, embedded in paraffin, sectioned at 4 m thickness, and stained with hematoxylin and eosin. One longitudinal section was obtained from each pair of lungs, and included the whole lungs and major airways. Slides were examined by a board-certified veterinary pathologist and bleeding was scored semiquantitatively: (0: absent, 1: minimal, 2: mild, 3: moderate, 4: marked).

Primary Mouse Tracheal Epithelial Cell Culture

Isolation and culture of primary mouse tracheal epithelial cell cultures (MTECs) were performed as previously described. Briefly, tracheas were washed with media, opened longitudinally, and then incubated in Ham's F-12 containing 3 mg/ml pronase for 18 hr at 4°C.

Cells isolated by enzymatic treatment were then seeded onto 0.4 μm pore size clear polyester membrane (Corning) coated with a collagen solution. At confluence, media was removed from the upper chamber to establish an air-liquid interface (ALI). Fully differentiated, 14-20 day-old post-ALI cultures were used for experiments.

For infection, the apical surface of MTEC cultures was washed extensively to remove accumulated mucins before inoculation with influenza A/X-31(H3N2) virus (MOI 10^{-6}). After incubation at 37°C for 1 hr, the virus inoculum was removed and the cultures were incubated in complete growth medium. Aliquots of the supernatants were collected at different time points for virus titration.

RNA was isolated from MTEC cultures by directly lysing the cells in the transwells, using the QIAGEN RNeasy mini kit, according to the manufacturer's instructions. Total RNA was reverse-transcribed using the ThermoScript RT-PCR System kit (Invitrogen). The cDNA served as template for the amplification of genes of interest and the housekeeping gene (*Hprt1*) by real-time PCR, using TaqMan Gene Expression Assays (Applied Biosystems), universal PCR Master Mix (Applied Biosystems) and the ABI-PRISM 7900 sequence detection system (Applied Biosystems). The fold increase in mRNA expression was determined using the $\Delta\Delta C_t$ method relative to the values in mock treated samples, after normalization to *Hprt1* gene expression. Virus was quantified by qPCR for the Matrix gene; primer sequences can be found in Table S3. Alternatively, virus was titrated on MDCK cells by the 50% tissue culture infective dose ($TCID_{50}$), by eight replicates of 10-fold serial dilutions, according to the Spearman-Karber method.

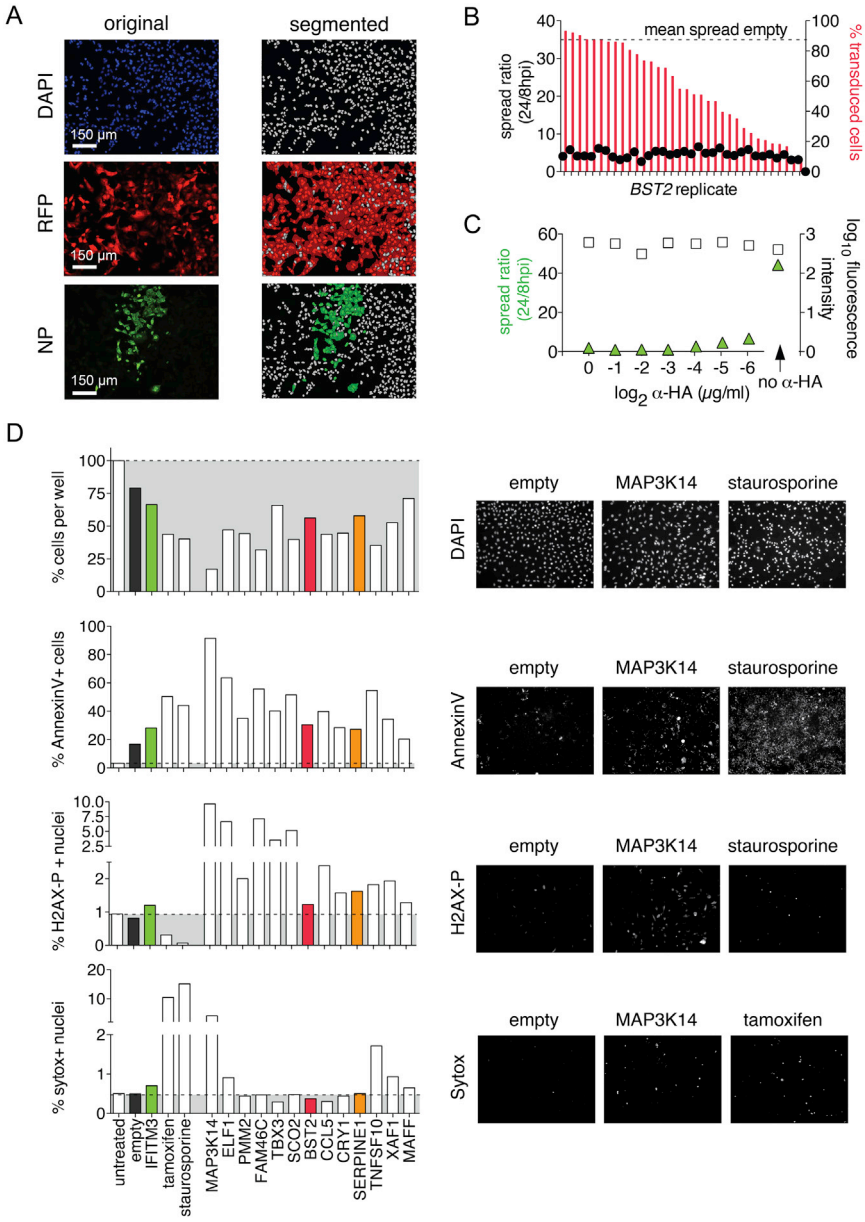

Figure S1. High-Throughput Microscopy Screens for Inhibitors of IAV Spread, Related to Figure 1

(A) Example of automated cell scoring from the HTM screen. Images show one representative out of 48 views per 96-well; original images from individual channels on the left (blue, DAPI-stained nuclei; red, transduced cells; green, NP-positive cells), and segmented images on the right (gray, nuclei; red, transduced cells; green, NP-positive cells).

(B) Establishing the spread ratio as a stable measure of spread over a large range of transduction efficiencies. A549 cells were transduced with a dilution series of *BST2*-expressing lentivirus, or a high dose of empty vector, the latter yielding 90% of transduced cells. A/WSN/33 spread was determined as described in Figure 1A.

(C) Establishing α-HA antibody to block IAV spread. A549 cells were infected with IAV WSN/33 for 24h, in the presence or absence of an α-HA antibody serial dilution, then fixed and stained for IAV NP. Shown are results from automated quantification, and representative images of two wells with the minimum inhibitory concentration, 0.125 µg/ml, or without α-HA are shown.

(D) Cytotoxicity assays of selected hits from the screen. A549 cells in 96-well plates were transduced with high-titer lentiviral stocks, yielding 90% transduced cells. Cells were then assayed by HTM for (from top to bottom): cell survival/proliferation, by DAPI stain and cell count; apoptosis, by Annexin V stain; DNA damage, by staining for phosphorylated H2AX; and cell membrane integrity, by Sytox stain. Tamoxifen and staurosporine were used as positive controls, untreated and untransduced cells as negative controls. Representative images from the respective assays are shown on the right.

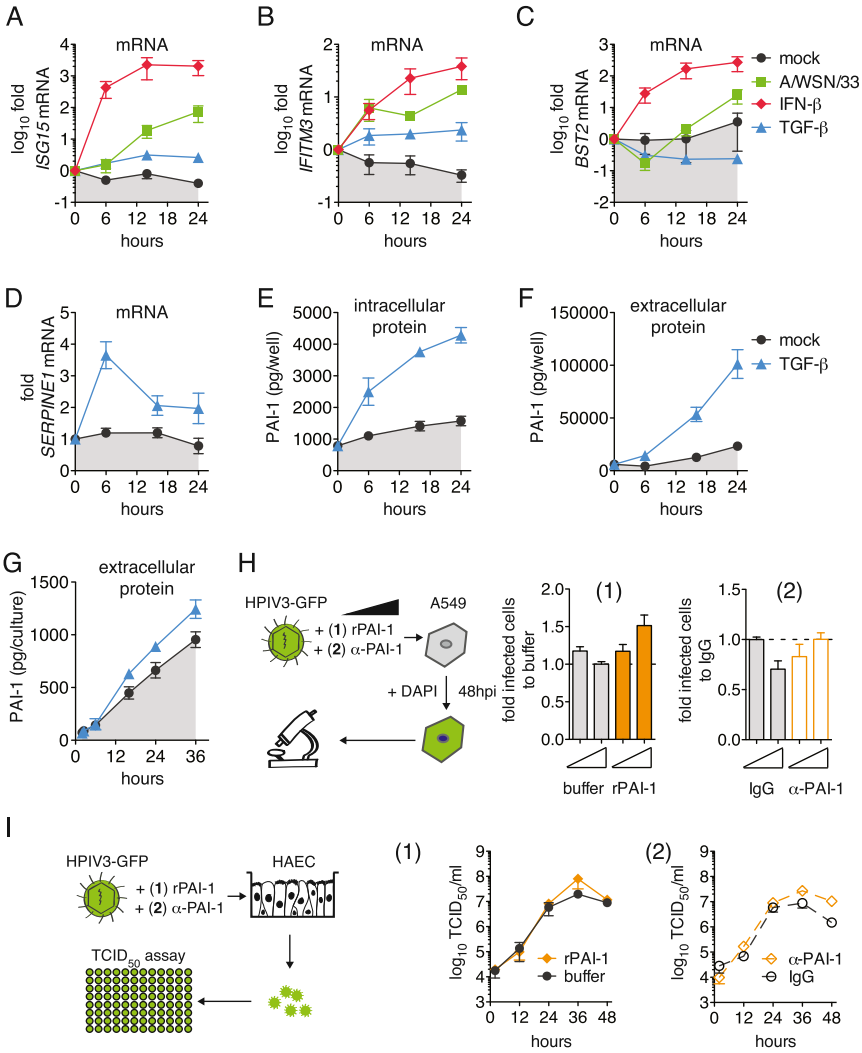

Figure S2. *SERPINE1* Gene Expression Profiles and the Role of Extracellular PAI-1 Protein in IAV Inhibition, Related to Figure 2

(A–C) Extended Figure 2A. *ISG15*, *IFITM3*, and *BST2* mRNA expression was normalized to housekeeping gene *RPS-11*, fold increase over pre-treatment control levels is shown.

(D–F) Extended Figure 2 A-C, showing the effect of TGF-β on *SERPINE1* mRNA expression (A), or on intracellular (B) and extracellular (C) PAI-1 protein levels. (G). Extended Figure 2D, showing the amount of extracellular PAI-1 protein levels from HAEC after induction with TGF-β. (H). A549 cells were infected with HPIV3-GFP for 48 hpi in the presence of either rPAI-1 (1) or α-PAI-1 antibody (2), and virus spread was assayed by HTM. The number of infected cells was normalized to buffer (1) or IgG control (2). Data are represented as mean ± SEM from n = 4 independent experiments. Statistical significance relative to empty control was determined by t tests. (I). HAEC were infected with HPIV3-GFP in the presence of either recombinant stable human PAI-1 (rPAI-1, 1) or α-PAI-1 antibody (2), and buffer (1) or IgG (2) as controls. Progeny virus was collected from apical washes at the indicated times and rPAI-1 or α-PAI-1 were replenished after each wash. Virus titers were determined by $TCID_{50}$ assay. Data are represented as mean ± SEM from n = 3 replicates.

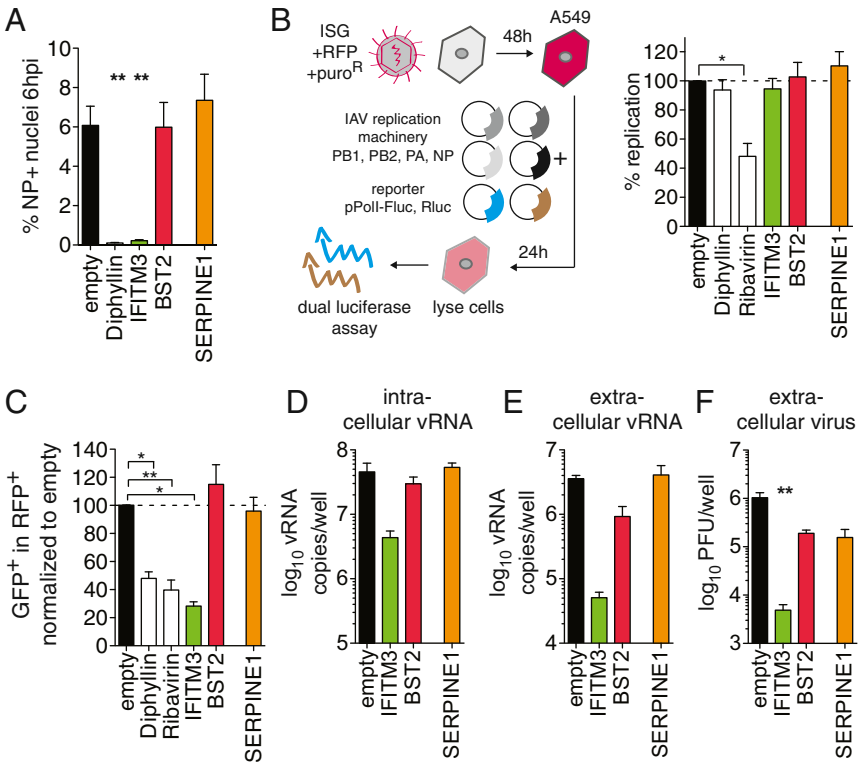

Figure S3. Effect of PAI-1 on Various Steps of the IAV Life Cycle

(A–E) A549 cells were transduced to express the indicated ISGs. Empty vector served as negative control, and the following positive controls were used: Diphyllin for IAV entry, Ribavirin for IAV replication. Data are represented as mean ± SEM from at least n = 4 independent experiments for all panels.

(A) Cells were challenged with IAV WSN/33 at MOI 1 and the number of NP-positive nuclei was determined at 6 hpi. Statistics by 1-way ANOVA and Dunn's multiple comparison test.

(B) IAV replication efficiency was assayed by a luciferase-based IAV minigenome assay. Expression constructs for components of the IAV replication machinery (PB1, PB2, PA and NP, of A/WSN/33 origin) were co-transfected with a reporter construct mimicking the viral genome, leading to expression of firefly luciferase (Fluc) when the genome mimic is replicated. Individual t tests compared to empty control.

(C) Influenza A/Puerto Rico/8/34-NS1-GFP virus replication during infection was assayed by FACS assay, determining the percentage of infected cells at 10 hpi (GFP-positive) in the ISG-overexpressing (RFP-positive) population. Statistical significance relative to empty control was determined by t tests.

(D–F) Cells were infected with IAV WSN/33 at MOI = 0.01. At 24 hpi, vRNA was extracted from cells (D) or supernatants (E), and vRNA copy number was determined by qRT-PCR. Infectious virus titers in supernatants at 48 hpi were determined by plaque assay on MDCK cells (F).

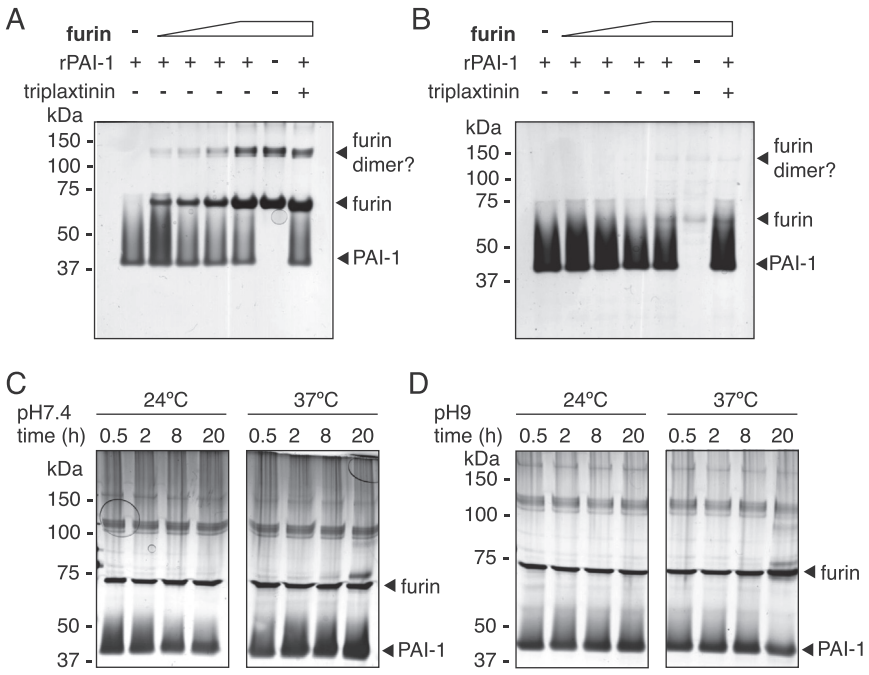

Figure S4. Protease Targets of PAI-1, Related to Figure 4

(A–D) Representative gel shift assays to test the formation of SDS-stable complexes of recombinant PAI-1 (rPAI-1) and furin. (A+B). 1μg of rPAI-1 was combined with increasing amounts of active recombinant furin (from abcam, A, and from NEB, B), and the mixture was separated on SDS gels followed by silver staining. Where indicated, Triplaxtinin was used at 3.3 mM to inhibit PAI-1. (C). To establish conditions for furin-rPAI-binding, 1μg rPAI was combined with 0.1 U furin (abcam) in 100 mM HEPES [pH 7.5], 1 mM $CaCl_2$, with the addition 0.5% Triton X-100 at either 24 or 37°C for indicated times.

(D) 1μg rPAI was combined with 0.1 U furin (abcam) in 100 mM HEPES [pH 9], 1 mM $CaCl_2$, with the addition 0.5% Triton X-100 at either 24 or 37°C for indicated times.

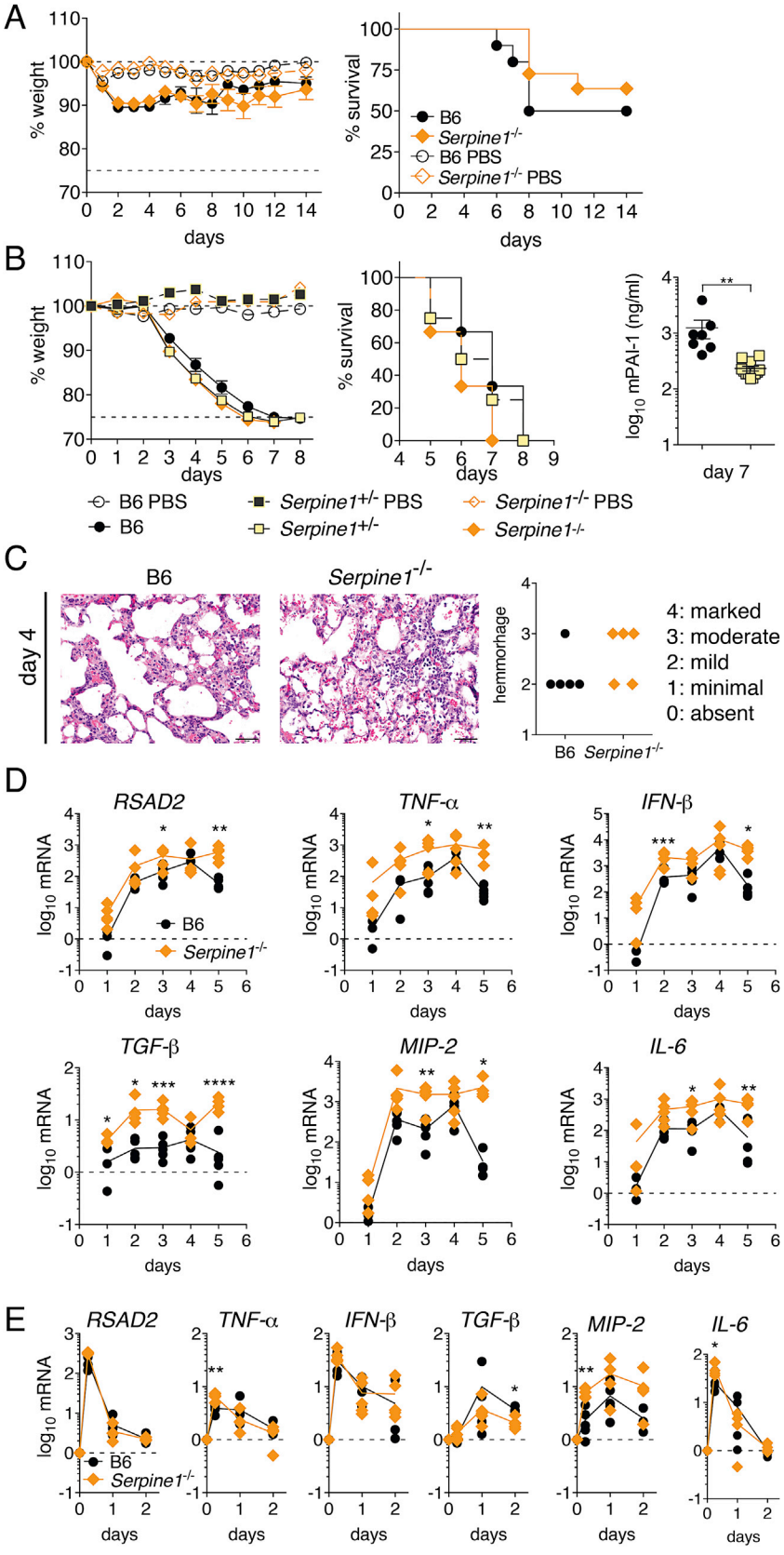

(legend on next page)

Figure S5. Role of *Serpine1* on Virus Infection in Mice, Related to Figure 6

(A) Wild-type (B6) or *Serpine1*$^{-/-}$ mice were infected intranasally with 1x10^5 PFU of vesicular stomatitis virus, and monitored for weight loss and survival. Data are represented as mean ± SEM from n = 10 infected B6 or *Serpine1*$^{-/-}$ mice, and n = 3 respective PBS control animals. Statistical significance was determined by individual t test or log rank test. No significant differences could be detected.

(B) Wild-type (B6), *Serpine*$^{+/-}$ or *Serpine1*$^{-/-}$ littermate mice were infected intranasally with 1000 PFU (36 LD_{50}) of influenza A/Puerto Rico/8/34 virus, and assayed for weight loss and survival. Homogenates of infected mouse lungs were assayed for mPAI-1 protein levels by ELISA.

(C) Pathology of lung cross-sections from mouse lungs at 4 dpi, stained with hematoxylin and eosin. Bar represents 50 μm. Severity of bleeding was scored quantitatively from n = 5 mice per group.

(D) Wild-type (B6) or *Serpine1*$^{-/-}$ mice were infected intranasally with 1000 PFU (36 LD_{50}) of influenza A/Puerto Rico/8/34 virus. Homogenates of infected mouse lungs were assayed for murine *RSAD2* (viperin), *TNF-α*, *IFN-β*, *TGF-β*, *MIP-2* and *IL-6* mRNA levels by qRT-PCR. n = 5 mice per group per day. Statistical significance between groups was determined by t tests.

(E) Wild-type (B6) or *Serpine1*$^{-/-}$ mice were challenged intranasally with 100μg poly(I:C). Homogenates of mouse lungs were assayed for murine *RSAD2* (viperin), *TNF-α*, *IFN-β*, *TGF-β*, *MIP-2* and *IL-6* mRNA levels by qRT-PCR. n = 5 mice per group per day. Statistical significance between groups was determined by t tests.